Estimating the variability of NO_x emissions from Wuhan with TROPOMI NO_2 data during 2018 to 2023

Qianqian Zhang[1], K. Folkert Boersma[2,3], Chiel van der Laan[4], Alba Mols[2], Bin Zhao[5,6], Shengyue Li[5,6], Yuepeng Pan[7,8]

[1]National Satellite Meteorological Center, Key Laboratory of Radiometric Calibration and Validation for Environmental Satellites, Innovation Center for Fengyun Meteorological Satellite (FYSIC), China Meteorology Administration, Beijing 100081, China
[2]Wageningen University, Environmental Science Group, Wageningen, the Netherlands
[3]Royal Netherlands Meteorological Institute, De Bilt, the Netherlands
[4]Eindhoven University of Technology, Eindhoven, the Netherlands
[5]State Key Joint Laboratory of Environmental Simulation and Pollution Control, School of Environment, Tsinghua University, Beijing 100084, China
[6]State Environmental Protection Key Laboratory of Sources and Control of Air Pollution Complex, Beijing 100084, China.
[7]Key Laboratory of Atmospheric Environment and Extreme Meteorology, Chinese Academy of Sciences, Beijing 100029, China
[8]College of Earth and Planetary Sciences, University of Chinese Academy of Sciences, Beijing 100049, China

Correspondence to: Qianqian Zhang, zhangqq@cma.gov.cn

Abstract. Accurate NO_x emission estimates are required to better understand air pollution, investigate the effectiveness of emission restrictions, and develop effective emission control strategies. This study investigates and demonstrates the ability and uncertainty of the superposition column model in combination with the TROPOspheric Monitoring Instrument (TROPOMI) tropospheric NO_2 column data to estimate city-scale NO_x emissions and chemical lifetimes and their variabilities. Using the recently improved TROPOMI tropospheric NO_2 column product (v2.4–2.6), ~~we~~ we derive daily NO_x emissions and chemical lifetimes over the city of Wuhan for ~~335~~ 372 ~~clear-sky~~full-NO_2-coverage days between May 2018 and December 2023, and validate the results with bottom-up emission inventories. ~~–~~We find insignificant weekly cycle of NO_x emissions for Wuhan. We estimate ~~a slight weekend reduction in NO_x emission with a weekend-to-weekday ratio of 0.95 and a small seasonal variation of NO_x emissions over Wuhan with~~ a summer-to-winter emission ratio of 0.~~87~~77, which is overestimated to some extent, though it is even higher provided by the bottom-up inventories. We calculate a steady decline of NO_x emissions from 2019 to 2023 (except for the valley in 2020 caused by the COVID-19 lockdown)~~, and the emission in 2023 is ~15% below the 2019 level,~~ indicating the success of the emission control strategy. ~~The estimated NO_x lifetimes range from 0.8 h (summer) to 5.3 h (winter), with an average of 2.6 h. Meanwhile, our method shows ~30% lower NO_x lifetimes for fast wind (> 7 m s^{-1}) speed.~~ The superposition model method results in ~~10~~15% lower estimation of NO_x emissions when the wind direction is from distinct upwind NO_2 hotspots compared to other wind directions, indicating the need to improve the approach for cities that are not relatively isolated pollution hotspots. The method tends to underestimate NO_x emissions and lifetimes when the wind speed is > 5—7 m s^{-1}, the estimation for Wuhan is ~4% for the emissions and ~8%

for the chemical lifetime. The results of this work nevertheless confirm the strength of the superposition column model in estimating urban NO_x emissions with reasonable accuracy.

1 Introduction

Nitrogen oxides ($NO_x \equiv NO_2 + NO$) are key atmospheric components affecting the formation of particulate matter and ozone (Bassett and Seinfeld, 1983; Jacob, 1999; Penner et al., 1991). They are emitted into the atmosphere mainly from the combustion of fossil fuels, which takes place primarily in urban areas, to heat and provide electricity to homes and businesses and to run cars and factories. Cities are responsible for more than 70% of global NO_x emissions, and this proportion increases with the process of global urbanization and industrialization (Park et al., 2021; Stavrakou et al., 2020; Baklanov et al., 2016). Thus, accurate NO_x emission inventories for cities are required for monitoring the effectiveness of reducing air pollution and for global and regional chemical models to reproduce the complicated urban air pollution (Beirle et al., 2011). Bottom-up city NO_x emission inventories are quite uncertain in the emission factors (Lu et al., 2015) and during the down-scaling from national or regional emissions to city level (Butler et al., 2008; Lamsal et al., 2011).

NO_2 has long been detected by remote sensing instruments with high quality because of its strong spectral features within the ultraviolet (UV)/visible spectrum~~,. and v~~Various satellite instruments have been providing tropospheric NO_2 column measurements for near-surface NO_x emissions estimation for tens of years (Burrows et al., 1999; Bovensmann et al., 1999; Levelt et al., 2006; Veefkind et al., 2012). Limited by the ~~early,~~ coarse spatial resolution of the early instruments, researchers computed the global or regional long-term mean NO_x emissions with satellite observations and chemical transport models (CTMs) (Martin et al., 2003; Lamsal et al., 2011; Kharol et al., 2015). With the improving capabilities of later satellite sensors, more researchers started to estimate NO_x emissions on higher spatial and temporal resolutions but still depended on CTMs (e.g., Ding et al., 2017; Visser et al., 2019; Xing et al., 2022). However, there are barriers to access and employment of CTMs, and there is a substantial computational burden when our target is a ~~single~~n individual city. Therefore, CTM-independent methods have been developed and applied to estimate NO_x emissions since the early 2010s (e.g., Beirle et al., 2011; De Foy et al., 2014; Kong et al., 2019; Beirle et al., 2019; Rey-Pommier et al., 2022).

Beirle et al. (2011) reduced~~otated~~ the 2-dimensional NO_2 map surrounding a large point source (such as a megacity or a power plant, factory) to the 1D NO_2 line density by integrating the NO_2 column density across the wind direction.~~toward the wind direction and integrated NO_2 columns perpendicular to the wind to obtain the so-called NO_2 line density along the wind direction.~~ They developed an Exponentially ~~Empirical~~ Modified Gaussian ~~model~~ method (EMG) to estimate ~~city~~ NO_x

emissions and ~~chemical~~ lifetime from the increase of NO_2 over the source~~city~~ and its decay downwind of the city. Over the years, ~~The~~ the model has been refined (Valin et al., 2013), validated (De Foy et al., 2014; 2015), applied (e.g., Lu et al., 2015; Lange et al., 2022; Goldberg et al., 2019) and extended (Liu et al., 2016; 2022). The EMG method~~odel~~ has been first applied to OMI NO_2 data to calculate NO_x emissions from cities, power plants, and factories across the globe and was shown to be accurate when wind speed is larger than 2 or 3 m s^{-1}. This method is frequently used to calculate mean NO_x emissions over longer time periods (like some years) with OMI data (e.g., Lu et al., 2015; Liu et al., 2016). ~~(Goldberg et al., 2019; Jin et al., 2021)In addition, this model requires a relatively large study area and is limited to calculating the mean NO_x emissions averaged over a longer time period.~~

At present, the much improved spatial resolution and retrieval quality of the TROPOMI sensor allows the quantification of episodic (like biomass burning) or even daily NO_x emissions with the EMG method (Goldberg et al., 2019; Jin et al., 2021). ~~makes it possible to track the NO_2 distribution and downwind plume over the city from a single satellite overpass.~~ Based on a single TROPOMI overpass, Lorente et al. (2019) ~~narrowed down the study area to the domain of one city and~~ developed a superposition column model to fit the NO_2 line density for daily NO_x emission~~s~~s. They found highest emissions on cold weekdays and lowest emissions on warm weekend days, indicating the significant contribution from home heating during winter in Paris ~~on (sub-)city scale~~. Zhang et al. (2023) used this model to estimate the daily variation of NO_x emissions over Wuhan from September 2019 to August 2020, and further inferred CO_2 emissions based on the simultaneous and co-located NO_2 and CO_2 satellite observations. The superposition column model estimates NO_x chemical lifetimes and emissions on daily basis, avoiding the bias ~~The superposition column model avoids the bias~~ caused by ~~the use~~using ~~of~~ the average ~~of~~d ~~the~~ NO_2 ~~product~~ columns in the nonlinear system ~~to calculate mean NO_x lifetimes and emissions~~ (Valin et al., 2013). However, Lorente et al. (2019) and Zhang et al. (2023) used daily hydroxyl radical (OH) concentration from CTMs as an important parameter, which induced computational burden when the study period is as long as several years. In addition, the CTM output OH concentration is highly uncertain (Zhang et al., 2021) and leads to uncertainty in the estimated city NO_x emissions and chemical lifetime.

In this study, we continue to focus on the city of Wuhan, extend our study period from May 2018 to December 2023, and estimate city NO_x emissions and lifetimes on a daily basis with the superposition column model. We discard CTM output OH concentration in the method to reduce the results' uncertainty and improve computing efficiency. Lorente et al. (2019); Zhang et al. (2023)Our purpose is, first, to demonstrate the ability of the superposition column model to provide information on city NO_x emissions and lifetimes on interannual, seasonal, and weekly variations influenced by changes in human activity; second, to investigate the model performance influenced by the meteorology (wind speed and directions). The rest of the paper is organized as follows: ~~Section~~ Section 2 introduces the data and methods we employ in this study. In ~~Section~~ Sect. 3, we compare our results with those of other studies, analyze the temporal variability of NO_x emissions and lifetimes over Wuhan, investigate the dependence of our estimations on the wind field~~, and~~. We discuss the uncertainties ~~in this work~~of this work in Sect. 4. The ~~conclusion~~ concluding remarks are presented in ~~Section~~ Sect. ~~4~~5.

2 Data and Material

2.1 TROPOMI NO_2 tropospheric columns

On 13 October 2017, the Copernicus Sentinel-5 Precursor (S-5P) satellite was successfully launched into a sun-synchronous orbit with the local overpass time at around 13:30. The TROPOspheric Monitoring Instrument (TROPOMI) is the only instrument on board S-5P, dedicated to air quality and climate monitoring. TROPOMI NO_2 columns are retrieved in the spectral range from ~~observes NO_2 at~~ 405~~–~~ to 465nm of the UV-visible spectral band with a~~n unprecedented~~ nadir spatial resolution of ~~3.5 × 5.5~~7.2 × 3.6 km^2 (reduced to 5.6 × 3.6 km^2 as of 6 August 2019) (Van Geffen et al., 2020; 2022). The small pixels and large swath width (approximately 2600 km) of TROPOMI allow the detection of localized point sources and downwind NO_2 plumes from cities on a daily basis (Beirle et al., 2019; Lorente et al., 2019).

This work uses the operational TROPOMI NO_2 version 2.4.0–2.6.0 algorithm from May 2018 to December 2023. Compared to the previous versions v1.x, ~~The~~ the version 2.3.1 includes a different treatment of the surface albedo to avoid negative and > 1 cloud fractions~~compared to the earlier versions~~, and updates the FRESCO-wide cloud retrieval that leads to a lowering cloud pressure. These result in~~which led to a~~ 10%~~~~–~~15~~40% increase of tropospheric NO_2 columns, depending on ~~over-polluted scenes~~the level of pollution and season (Van Geffen et al., 2022; Lange et al., 2023). There is a major change from version 2.3.1 to 2.4.0. In v2.4.0, a new TROPOMI surface albedo climatology (Directional Lambertian Equivalent Reflectivity, DLER) was implemented in the cloud fraction and cloud pressure retrievals and air-mass factor calculation (Eskes et al., 2023). The use of the DLER results in a substantial increase of NO_2 columns in vegetated regions, and the higher resolution (0.125 ° × 0.125 °) of the DLER better resolves the variability in the surface albedo (Keppens and Lambert, 2023). The ~~v2.4.0~~ version 2.4.0 made a complete mission reprocessing from 1 May 2018 to 22 July 2022 and then switched to the offline mode. ~~until 12 March 2023.~~ The version 2.5.0 implemented a minor bug fix concerning the qa_value field over snow or ice-covered regions. The version 2.6.0 started on 16 November 2023, and is exactly the same as version 2.5.0.

The version 2.4.0–2.6.0 Level 2 tropospheric NO_2 products are reported to be biased between +33% (over cleaner areas) and –50% (over highly polluted areas) compared to the ground-based MAX-DOAS data from 29 stations, with the overall negative median bias being 28%. Amongst all the 29 ground stations, one is in north China, Xianghe. At Xianghe, the TROPOMI tropospheric NO_2 columns correlate (R^2 = 0.88) well with the MAX-DOAS data with a median low bias of ~20%, and the weekly averaged relative difference is within ±30% for most of the days (Keppens and Lambert, 2023). When we use the TROPOMI data in Wuhan, some low bias is expected, and we adjust a scale factor of 1.2 to (partly) correct the bias and screen each ground pixel for the quality assurance flag (qa_value) greater than 0.75.

2.2 Wind data ~~and chemical parameters~~

Apart from the tropospheric NO_2 columns, wind field (wind direction and wind speed) ~~and atmospheric chemical parameters are~~is needed as forward model parameters to determine city NO_x emissions and chemical lifetimes. We use the reanalysis ~~of~~

~~hourly~~ wind data on pressure levels provided by the fifth-generation (ERA5) European Center for Medium-Range Weather Forecasts (ECMWF) (Hersbach et al., 2020). This dataset provides hourly wind data on 37 vertical levels with the~~has a~~ horizontal resolution of 0.25 ° × 0.25 °~~,~~. Considering the vertical consistency of wind speeds and directions, ~~and~~ we use the 3 levels mean meridional and zonal wind below 950hPa.~~ ~~The two hourly values immediately before and after the TROPOMI overpass timestamp are linearly interpolated.

~~The chemical parameters, including the hydroxyl radical (OH) concentration and atmospheric NO_x/NO_2 ratio, are obtained from version 12.3.2 GEOS-Chem chemical transport model simulations for lack of observations. The nested grid version of the GEOS-Chem model over East Asia (70 ℃—140 ℃, 15 ℃—55 ℃) operates full-aerosol-oxidant simulation at 0.25 ° × 0.3125 °spatial resolution with 47 vertical levels from ground to the top of the stratosphere (Zhang et al., 2015). The GEOS-Chem model is widely used and refined worldwide to simulate and evaluate the atmospheric aerosol and gas phase pollutants (https://geoschem.github.io/overview.html). It has been extensively found to be skillful in simulating the concentration and distribution of ozone, $PM_{2.5}$, and nitrate aerosols in China (Zhai et al., 2021; Geng et al., 2017; Lu et al., 2019; Li et al., 2019). Thus we can say that the GEOS-Chem model produces compelling predictions of chemical parameters of NO_x. This work uses the boundary layer mean OH concentration at 12:00–14:00 to predict prior values for the atmospheric NO_x chemical loss rate. As we stated in our previous work (Zhang et al., 2023), the GEOS-Chem simulated NO_x/NO_2 ratio varies less than 10% with seasons, so we use the fixed value of 1.26 in this work following Zhang et al. (2023).~~

2.3 Emission inventory

An ~~I~~initial guess of NO_x emission patterns and amounts are needed in this study, and we use the Air Benefit and Attainment and monthly Cost Assessment System Emission Inventory (ABACAS-EI) (Zhao et al., 2013; Zhao et al., 2018; Zheng et al., 2019) for the year 2019 to provide this information. The ABACAS-EI is available at 1km × 1km gridded resolution over China, and it is developed based on activity rates and energy consumption levels with an estimated uncertainty of ±35% (Zhao et al., 2013; Li et al., 2024b). Two other bottom-up NO_x emission inventories are also used for comparison. The first one is the Emission Database for Global Atmospheric Research (EDGAR) v8.1, which provides monthly sectoral 0.1 ° × 0.1 ° NO_x emissions from 2000 to 2022, and the 2018—2022 data are employed. The second is the 2018—2020 monthly NO_x emission from the Multi-resolution Emission Inventory model for Climate and air pollution research (MEIC) v1.4, with the spatial resolution of 0.25 ° × 0.25 ° (Zheng et al., 2021a; 2021b)~~The Emission Database for Global Atmospheric Research (EDGAR) v6.1 of 2018 annual total is also used for comparison~~.

2.4 The superposition column model

Lorente et al. (2019) introduced this superposition column model to estimate city NO_x emissions and chemical lifetimes based on a single TROPOMI overpass and determined daily NO_x emissions over Paris. Zhang et al. (2023) modified and used this model for the Chinese city of Wuhan in a more polluted background.

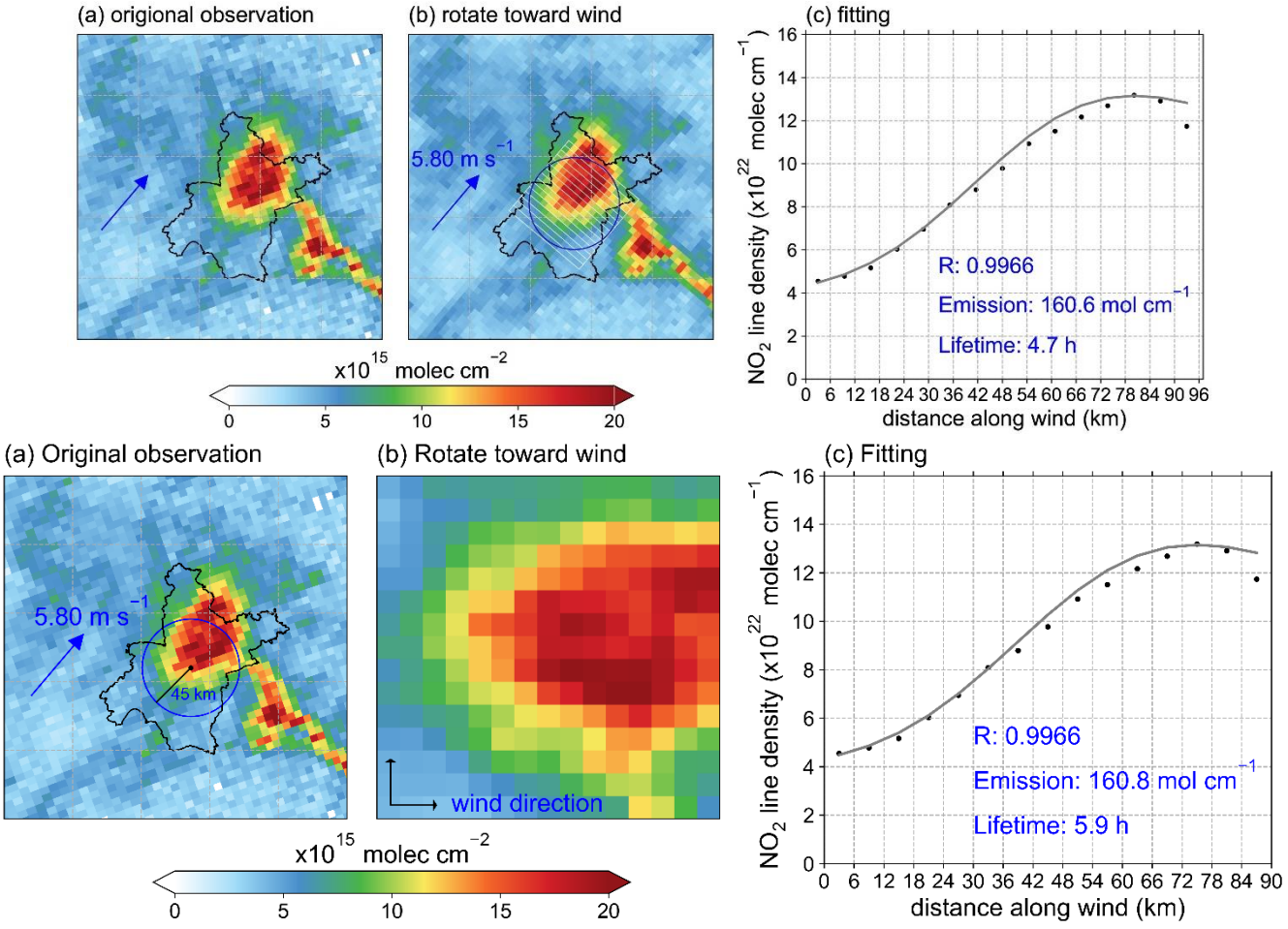

Figure 1: The analysis steps of the superposition column model. (a) The original TROPOMI NO_2 columns ~~were~~ are on 4 March 2023. The administrative boundary of Wuhan is plotted, and ~~T~~the blue circle inside denotes the study domain centered on Wuhan city center (114.4 °E, 30.6 °N) with a 45 km radius.~~, and the white lines indicate the grid cells along with the wind direction.~~ (b) NO_2 columns resampled at a grid map aligned with the wind direction within the study domain. ~~The blue circle inside denotes the study domain centered on Wuhan city center with a 45 km radius, and the white lines indicate the grid cells along with the wind direction.~~ (c) ~~Integrate t~~The grid cells perpendicular to the wind direction are integrated to obtain the NO_2 line density and fit it with the superposition column model.

Using the day 4 March 2023 as an example, we demonstrate the analysis steps of the superposition column model (Fig. 1). We focus on the build-up of NO_2 columns over a 45 km radius around the city center 114.4 °E, 30.6 °N, which covers the urban area of Wuhan~~of Wuhan city center~~ (the blue circle in Fig. ~~1b~~1a). Compared to Zhang et al. (2023), our study domain is limited to the urban area (within the Fourth Ring Road) of Wuhan. For one reason, most (~ 60%) of the NO_x emissions are concentrated in the urban area (Zhang et al., 2023); for another, we use regional mean wind fields and NO_x chemical loss rate,

the larger study domain would induce large uncertainty in the result. We construct a 15 × 15 grid map centered at the city center with each grid size of 0.05 ° × 0.05 ° (6km × 6km), and rotate the grid map toward the mean wind direction. One demission of the grid map is along with and the other perpendicular to the wind direction. The mean wind direction is determined by the mean meridional and zonal winds over the study domain. The original TROPOMI observation (Figure Fig. 1a) is sampled into the rotated grid map (Fig. 1b). The TROPOMI NO_2 columns in the 15 grid cells perpendicular to the wind direction are integrated to form the so-called NO_2 'line densities' (Beirle et al., 2011), resulting in 15 grid cells along the wind direction (Fig. 1c).

Then, the NO_2 line density is fitted with the superposition column model (Lorente et al., 2019; Zhang et al., 2023) which is based on a simple column model (Jacob, 1999). We solve each grid cell along the wind direction with a the simple column model, NO_x NO_2 builds up within the current cell and decays exponentially downwind of this cell.

$$N_i(x) = \frac{E_i}{k}\left(1 - e^{-kL/u}\right) \cdot e^{-k(x-x_i)/u} \cdot \frac{[NO_2]1}{[NO_x]/[NO_2]} \quad for\ x > x_i \quad , \tag{1}$$

$$N_i(x) = 0 \qquad for\ x \le x_i \ , \tag{2}$$

$$N(x) = \sum_{i=1}^{n} N_i(x) + b + \alpha x \tag{3}$$

NO_x emissions from cell i (E_i, mol cm^{-1} s^{-1}) along the wind direction contribute ($N_i(x)$, mol cm^{-1}) to the overall line density through the build-up of NO_x NO_2 within the current cell and exponential decay in the downwind cells (Eq. (1)). We assume a first-order loss of NO_2 reacted with OH in the atmosphere. In Eq. (1), k (s^{-1}) represents the loss rate of NO_2 at the TROPOMI overpass time., and the relationship between k and NO_2 chemical lifetime $\tau_{[NO_2]}$ (h) is $k = \frac{1}{\tau_{[NO_2]} * 3600}$. Here, Lorente et al. (2019); Zhang et al. (2023) we make an initial guess to the NO_2 chemical lifetime of 4 h for cold seasonmonths (October to March) and 2 h for warm monthsseason (April to September) to derive the parameter k. We set a large range for k to allow it to change between 1/4 to 4 times of the initial value. k is determined by the atmospheric OH concentration ($[OH]$, molec cm^{-3}), the reaction rate constant k' between NO_2 and OH (here we use 2.6 × 10^{-11} cm^3 molec^{-1} s^{-1} from the GEOS-Chem model) and the NO_x/NO_2 ratio in the atmosphere: $k = \frac{k'[OH]}{[NO_x]/[NO_2]}$. L denotes the length of each grid cell, i.e. 6 × 10^5 cm, and u is the wind speed (cm s^{-1}). We follow Zhang et al. (2023) to take a fixed value 1.26 for $[NO_x]/[NO_2]$. E_i has makes no contribution to the its upwind cells (Eq. (2)).

The contributions from all the 15 cells are stacked up to ~~make~~ construct the superposition column model, and combined with the contribution from the background NO_2 line densities ($b + \alpha x$) to obtain the overall $N(x)$ (Eq. (3)). The initial guess of the background value b is set as the NO_2 line density at the ~~upend~~ upwind end point $N(0)$.

The terms E_i, k, ~~and~~ α and b are fitted through a least squares minimization to the TROPOMI observed NO_2 line densities ($N_{TROPOMI}(x)$) and the a priori ABACAS NO_x emissions ($E_{ABACAS,i}$) to determine $N(x)$. The cost function is defined as follows:~~the combination of a least squares minimization of $N(x)$ to the TROPOMI observed line density $N_{TROPOMI}(x)$ and E_i to the ABACAS EI NO_x emissions $E_{ABACAS,i}$~~

$$\text{func} = \left(\frac{N(x)-N_{TROPOMI}(x)}{N_{TROPOMI}(x)}\right)^2 + fac\text{~~tor~~} * \left(\frac{E_i-E_{ABACAS,i}}{E_{ABACAS,i}}\right)^2 \quad (4)$$

The emission term is used in the cost function to ~~dilute~~reduce the dependence of fitted NO_x chemical lifetimes and emissions on the $\tau_{[NO_2]}$, for too large a varying range is applied for it. We exert a scale factor (fac) changing between 0.1 and 0.2 to the emission term to make sure the cost function is dominated by the NO_2 line density term.~~OH concentrations, which are of significant uncertainty and have no solid observations~~ (!!! INVALID CITATION !!! (Zhang et al., 2021)).~~Zhang et al. (2023)~~

Finally, ~~In the fitting procedure, we make some changes compared to Zhang et al. (2023). First, for the treatment of the initial guess of OH concentrations, considering the uncertainty in simulated OH concentrations, we use the monthly instead of daily mean noon time (12:00－14:00) boundary layer OH concentration as the initial guess for the daily inversion. We allow it to change between 0.3 to 2 times in lieu of the ±30% interval around the initial value; this range is chosen because most (more than 90%) of the simulated daily OH concentration falls in the 0.3 to 2 times the monthly mean value. Second, the combination of a least squares minimization of $N(x)$ to the TROPOMI observed line density $N_{TROPOMI}(x)$ and E_i to the ABACAS EI NO_x emissions $E_{ABACAS,i}$ (Eq.(4)). We restrict the emissions to a gaussian shape and a scale factor is applied to the emission term. It is found to be ~0.1 for all the days that lead to the best fit of the NO_2 line densities. We make these modifications to the superposition column model because we are trying to dilute the dependence of fitted NO_x emissions on the OH concentrations, which are of significant uncertainty and have no solid observations (Zhang et al., 2021).~~

~~$$\text{func} = \left(\frac{N(x)-N_{TROPOMI}(x)}{N_{TROPOMI}(x)}\right)^2 + factor * \left(\frac{E_i-E_{ABACAS,i}}{E_{ABACAS,i}}\right)^2 \quad (4)$$~~

~~(4)~~the total NO_x emissions E (in the unit of mol s^{-1}) from the study domain can be calculated with

$$E = \sum_{i=1}^{15} E_i \times L \quad (5)$$

and the estimated NO_x ($\tau_{[NO_x]}$) chemical lifetime is obtained through Eq.(6) (Seinfeld and Pandis, 2016):

$$\tau_{[NO_x]} = \frac{1}{k \cdot 3600} \cdot \frac{[NO_x]}{[NO_2]} \quad (6)$$

3 Results ~~and discussion~~

3.1 Mapping Wuhan's NO_x emissions and ~~comparison to other inventories~~chemical lifetimes

From May 2018 until December 2023, we collect 581 overpasses with ~~clear skies~~full-NO_2-coverage over Wuhan. We remove the overpasses with inhomogeneous wind fields, which happen most frequently in winter. The inhomogeneous wind fields include the situations when the wind direction changes more than 45° within 2 hours before the satellite overpasses, and the wind at zonal or meridional direction reverses at different pressure levels when the satellite overpasses. Multiple overpasses within one day are analysed separately to calculate NO_x emissions and then averaged for the daily mean emission level. ~~We also exclude the days with estimated NO_x emissions beyond 0.5—1.5 times the ABACAS bottom-up emissions. The 0.5—1.5 times interval is chosen because it covers the uncertainty level of bottom-up NO_x emissions, the degree of seasonal and weekly variability, and the year-to-year change of NO_x emissions over Wuhan from 2018 to 2023. This standard is not applied when calculating NO_x emissions during the COVID-19 lockdown influenced period (23 January 2020 to the end of April 2020).~~

Finally, we obtain a total of 3723~~5~~ days with valid NO_x emissions and chemical lifetimes estimations. The number of valid days for each year and each season are summarized in Table 1. For the five years (2019—2023) with full-year measurement, the percentage of days with valid estimations is 1~~4.0~~5.3%—~~19.2~~22.5%. Seasonally, we obtain the most valid days in autumn (defined as September to November), followed by summer (June to August). There are least valid days in winter (December to February) ~~after spring (March to May) for~~due to the cloudy and polluted conditions ~~in winter~~.

Table 1: Number of days with valid NO_x emissions and lifetime estimations for each year and each season.

By year	2018	2019	2020	2021	2022	2023
	2~~8~~6	69~~64~~	5~~6~~9	65~~65~~	82~~70~~	72~~51~~
By season[a]	Spring		Summer	Autumn		Winter
	82~~70~~		70~~1~~	131~~19~~		62~~50~~

a. The COVID-19 lockdown-influenced days (23 January to the end of April in 2020) are not considered when we count the valid days by season.

3.1.1 NO_x emissions

Zhang et al. (2023) used the superposition column model to calculate NO_x emissions over Wuhan for the period from September 2019 to August 2020. They calculated 11.5 kg s^{-1} (equivalent to about 250 mol s^{-1}) NO_x emissions over Wuhan (including the ~~city center~~urban area and the outskirts of Wuhan) from September to November 2019. We estimate 1~~53.4~~48.8 ± 4~~0.5~~8.8 mol s^{-1} NO_x emissions over the ~~central~~ urban region of Wuhan for the same period, indicating ~60% of NO_x emissions are concentrated over the central area. Lange et al. (2022) applied the EMG ~~function~~ method to calculate NO_x

emissions over Wuhan from March 2018 to ~~November~~ January 2020 ~~(the COVID-19 lockdown-influenced period excluded)~~ of 115.1 ± 10.1 mol s^{-1}~~2~~, and they used ~~a~~ much earlier TROPOMI data versions 1.1.0−1.3.0 with larger low bias and they did not apply an ad hoc correction factor of 1.2 as we do in this study. ~~Zhang et al. (2023) estimated an average NO_x lifetime over Wuhan of 2.46 h, Lange et al. (2022) reported a 2.94 ±0.3 h. This study calculates a mean NO_x lifetime of 2.61 h, close to the previous studies.~~

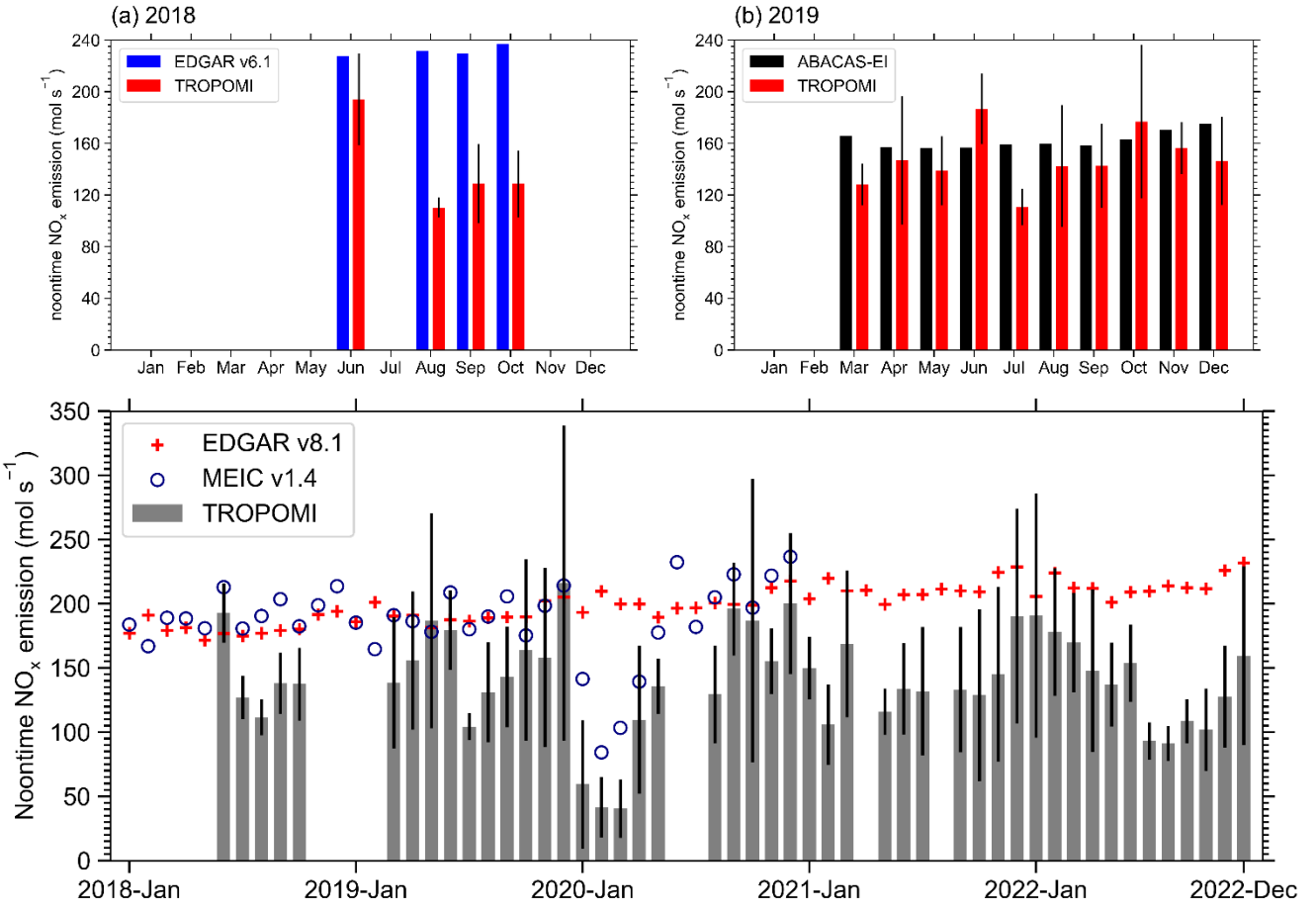

Figure 2: Monthly NO_x emissions estimated with the TROPOMI data (~~red~~grey columns), reported by EDGAR ~~v6~~v8.1 (red ~~pluses~~blue) and ~~ABACAS-EI~~MEIC v1.4 (~~black~~blue circles)~~ from 2018 to 2022 (from 2018 to 2020 for MEIC v1.4)~~~~for (a) 2018 and (b) 2019~~. The emissions of EDGAR v8.1 and MEIC v1.4 are scaled to the noontime emission intensities to keep in consistent with TROPOMI. The TROPOMI monthly mean is calculated only when three or more days are available. Thus, the comparison is unavailable~~s are only possible~~ for ~~some~~ several months. The error bars on the TROPOMI estimations represent the standard deviation of the daily NO_x emissions in each month~~ derived by the superposition column model~~.

We now compare the NO_x emissions over Wuhan estimated in this study with those from ~~ABACAS-EI (for the year 2019) and~~ EDGAR ~~v6~~v8.1 ~~(for the year 2018)~~and MEIC v1.4 in ~~Figure~~ Fig. 2. The monthly ~~It needs to be pointed out that the~~

~~annual~~ total NO_x emissions are provided in the ~~ABACAS-EI and~~ EDGAR ~~v6~~v8.1 and MEIC v1.4, and we convert them into monthly mean noontime emission intensities with the time factor in ABACAS-EI. Since the monthly mean TROPOMI NO_x emissions are calculated only when three or more days' NO_x emissions are available, ~~we obtain only four months (June, August, September, and October) in 2018 and 10 months (March to December) in 2019~~the comparison is missing for the months November 2018 to February 2019, June and July 2020, April and August 2021. Overall, the TROPOMI estimation is close to the bottom-up emission inventories during cold months, while much lower during warm months. For the three years (2018 to 2020) when MEIC v1.4 data is available, the difference between TROPOMI and MEIC v1.4 is within 35%, and both of them capture the NO_x emission reduction in early 2020 due to COVID-19 lockdown. TROPOMI and EDGAR v8.1 are close to each other (within 30% difference) in 2018 and 2019, but the discrepancy is larger since 2020. EDGAR v8.1 is > 50% higher than TROPOMI from 2020 to 2022.~~For 2018, we estimate monthly NO_x emissions over Wuhan of ~140.5 mol s^{-1}, while it is as high as ~230 mol s^{-1} estimated by EDGAR v6.1. Lange et al. (2022) also found a large discrepancy between satellite-derived and EDGAR bottom-up NO_x emissions over Wuhan and several other large cities. For 2019, the monthly NO_x emissions over Wuhan calculated by the superposition column model is ~4.7% lower than that from the ABACAS-EI, close to the difference reported by Zhang et al. (2023).~~

3.1.2 NO_x chemical lifetimes

Different from Lorente et al. (2019) and Zhang et al. (2023), we do not use the CTM simulated daily OH concentration to constrain city NO_x chemical lifetime, instead we fit it around an initial value. The initial guess of the chemical lifetime for cold and warm months are determined according to the fitting results of Zhang et al. (2023).

~~We~~

~~Zhang et al. (2023) estimated an average NO_x chemical lifetime over Wuhan of 2.46 h, Lange et al. (2022) reported a 2.94 ±0.3 h. This study calculates a mean NO_x lifetime of 2.61 h, close to the previous studies.~~

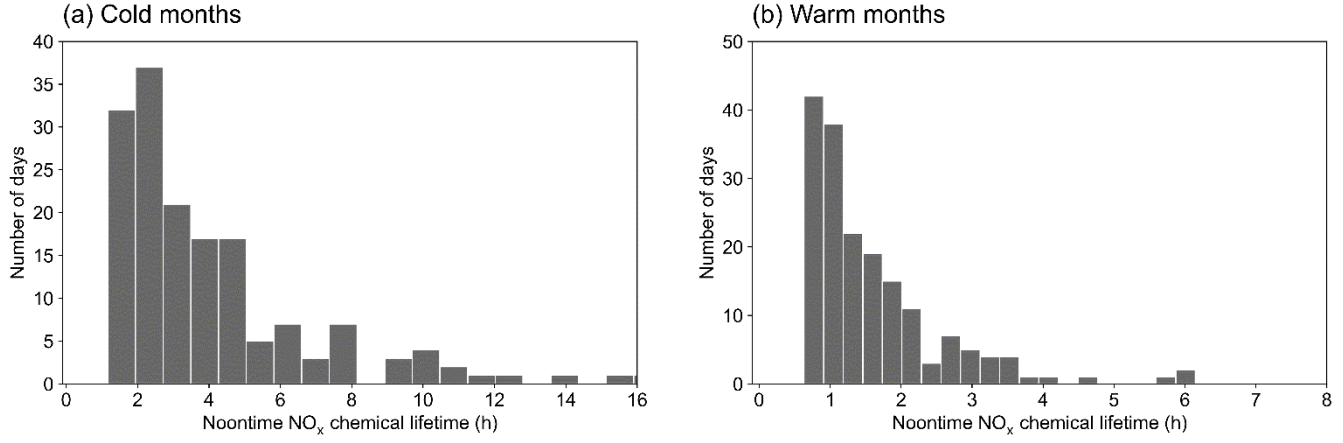

Figure 3: Distribution of estimated NO_x chemical lifetimes over Wuhan in (a) cold months and (b) warm months.

The final generated NO_x chemical lifetime over Wuhan is displayed in Fig~~ure~~. 3. Overall we calculate a mean NO_x chemical lifetime of 2.4820 h, close to the 2.46 h estimated by Zhang et al. (2023), ~~but~~and is around ~~20~~5% lower than Lange et al. (2022) reported 2.94 ±0.3 h for the NO_x effective lifetime. ~~Lange et al. (2022)~~ The fitting result~~Our initial guess~~ for cold months NO_x chemical lifetime is ~~4 h(Seinfeld and Pandis, 2016), and the fitting result is 3.44~~.25 h, ~~lower than the initial guess,~~ and for most of the days, the estimated NO_x chemical lifetime is between 1.5 h and ~~4~~6 h. For the warm months, most of the estimates are within the 0.~~5~~8 – 2.5 h range, and the mean value is 1.62 h~~is also lower than the initial guess~~.

3.2 Temporal variability of NO_x emissions over Wuhan

Considering the atmospheric photochemical activity of NO_x, previous studies using the build-up of NO_2 pollution along the wind direction are primarily based on satellite NO_2 data in the warm ~~season~~ months~~(May to September in the Northern Hemisphere)~~ (Lu et al., 2015; Liu et al., 2016; Goldberg et al., 2021b). Lange et al. (2022) have ~~proven~~ proved that it is also possible to fit the NO_2 line densities for NO_x emissions and lifetimes in winter when NO_x lifetimes are much longer. Zhang et al. (2023) estimated a year-round daily NO_x emissions and lifetimes over Wuhan from September 2019 through August 2020. In this study, we extend the study period to 6 years. We have more than 40 valid days for each ~~weekday and weekends~~day of the week, and more than ~~50~~ 60 days for each season and each year (2018 excepted), making it possible to investigate the time variabilities of NO_x emissions over Wuhan on the weekly, seasonal, and interannual scales.

3.2.1 Weekly cycle

To identify the weekly cycle of NO_x emissions over Wuhan, we exclude the ~~25~~ 27 valid days during the COVID-lockdown period, resulting in ~~310~~ 345 valid daily NO_x emission estimates~~s~~. The weekend effect (defined as the reduction in NO_2 columns or NO_x emissions on weekends compared to weekdays) is widely recognized and reported in cities around the world but not in Chinese cities (Beirle et al., 2003; Stavrakou et al., 2020; Zhang et al., 2023; Goldberg et al., 2021a). Beirle et al. (2003) explained the absence of a weekend effect in Chinese cities by the dominant role of power plants and industry in NO_x emission sources. Stavrakou et al. (2020) found a slight reduction of NO_2 columns on weekends compared to the weekday average in Chinese cities from 2005 to 2017. Because of China's clean air action on power plants and the growing vehicle population, transportation has replaced power plants as the dominant contributor to NO_x emissions. However, we still find no significant ~~minimum~~ reductions on weekends for Wuhan, as shown in ~~Figure~~ Fig. ~~3~~4. Wei et al. (2022) also reported weak weekday/weekend differences in surface NO_2 concentration over Chinese cities. The 'Annual Report on Wuhan Transportation Development (2023)' (https://jtj.wuhan.gov.cn/znjt/zxdt/202409/t20240904_2450210.shtml, last access: 25 November 2024, in Chinese) revealed that the traffic flow passed through the Outer Ring Road and the Fourth Ring Road of Wuhan was highest on Friday and lowest on Tuesday and Sunday, but the difference is only less than 2%. Our result also sees an insignificant maximum on Friday and minimum on Tuesday. Cultural and living differences with other cities might

explain the absence of a strong weekend effect in Wuhan. Shops, restaurants, and traffic are much busier on weekends, especially at noon when the satellite passes. Lange et al. (2022) reported a 0.79 weekday-to-weekend ratio for Wuhan, the possible reason is that our study is limited to the urban area, while a larger area is needed by Lange et al. (2022) to perform the EMG method. The different behaviors and sources in the urban and suburban areas might lead to the different weekend-to-weekday emission ratio.

~~We calculate an overall 0.95 weekend-to-weekday NO_x emission ratio, while Lange et al. (2022) reported the ratio of 0.79. We do not have a clear explanation for this difference. Actually, we find a NO_x emissions maximum on Thursday, which was also seen by Beirle et al. (2003) for Chinese cities. The weekday maximum is mostly seen on Fridays or Thursdays in cities in Europe and North America(Stavrakou et al., 2020; Goldberg et al., 2024).~~

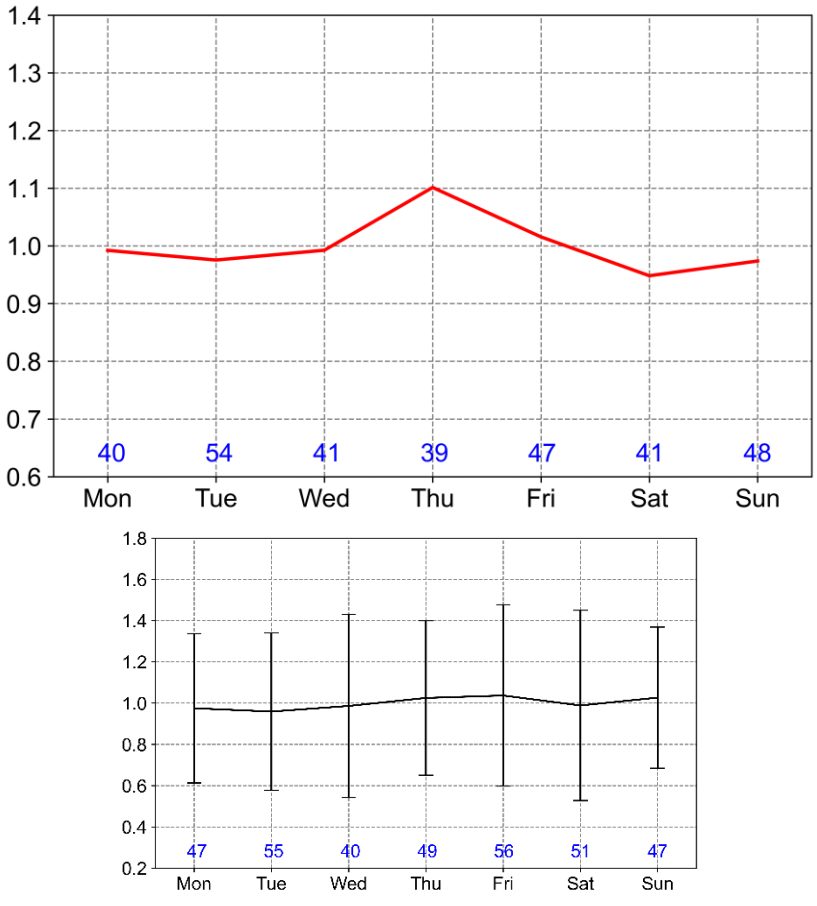

Figure ~~3~~4: Weekly cycle of mean (2018—2023) NO_x emissions. The emissions are normalized with respect to the mean emissions of all the days. The number of valid measurement days for each ~~weekday and weekends~~day of the week is listed in the plot. The error bars represent the standard deviation of the daily NO_x emissions.

3.2.2 Seasonal pattern

Seasonal NO_x emissions over Wuhan are plotted in ~~Figure~~ Fig. ~~4a~~5a. ~~Similar O~~to the bottom-up emission inventories, our results reveal that Wuhan NO_x emissions vary ~~little variability in NO_x emissions between seasons~~from season to season with the highest emission in winter and lowest in summer. Winter emissions are ~~slightly~~ higher by ~~10.5~~9.6%—~~14.5~~29.4% than the other three seasons. This is different from the bottom-up emission inventories which show little seasonal difference, as shown in Fig. 2. According to the bottom-up emission inventories, a small seasonal variation of NO_x emissions should be expected, ~~This is expected,~~ for transportation and industry are the two dominant contributors to NO_x emissions over Wuhan, making up nearly 90% of the total NO_x emissions, and these two emission sectors exhibit no significant seasonal variations (Zheng et al., 2018). Also, Wuhan is located in central China where winter is mild, and there is no domestic heating in winter. The summer-to-winter NO_x emission ratio usually serves to indicate the relative importance of winter heating and summer power consumption due to air conditioning. Here we calculate a summer-to-winter ratio of 0.~~87~~77, ~~while~~ and Lange et al. (2022) reported an even lower 0.3, while it is larger than 0.85 in the bottom-up emission inventory.

Two possible factors may contribute to the large difference in the summer-to-winter emission ratio between this study and Lange et al. (2022). First is the different treatment to the NO_x-to-NO_2 ratio. We use a fixed NO_x-to-NO_2 ratio of 1.26, while Lange et al. (2022) calculated the ratio from day to day, and it was lower in summer than in winter, leading to a lower NO_x emission estimation in summer. ~~(Seinfeld and Pandis, 2016)~~Second is that we use the bottom-up emission inventory to constrain our estimation, the flat seasonality of the bottom-up emissions leads to a higher summer-to-winter ratio of this study.~~. Their much lower summer to winter emission ratio may be caused by much lower estimated summertime NO_x emissions or much higher winter emissions or both.~~

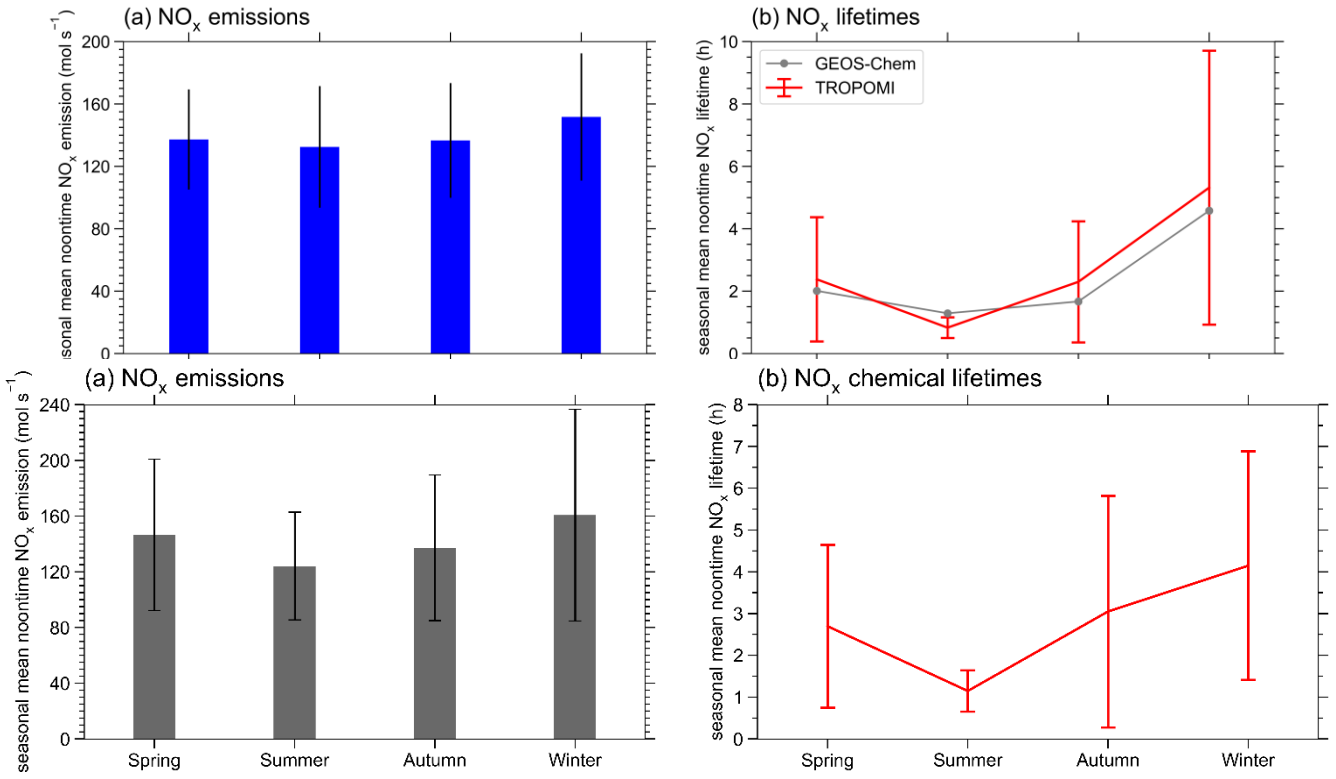

Figure 45: ~~(a)~~ TROPOMI estimated seasonal mean noontime (a) NO_x emissions and (b) chemical lifetimes over Wuhan. ~~(b) TROPOMI estimated (red line), and GEOS-Chem model produced (gray line) seasonal mean noontime NO_x lifetimes over Wuhan.~~ The error bars represent the standard deviation.

~~Determined~~ Dominated by the NO_x photochemical activity rate under the influence of temperature and OH concentrations, the NO_x chemical lifetimes are longest in winter and shortest in summer, as shown in ~~Figure~~ Fig. ~~4b~~5b. Spring and autumn NO_x chemical lifetimes are close to each other between winter and summer. For winter, we estimate an average of 4.1 h, close to the 4.8 h reported by Zhang et al. (2023), and longer than the ~3 h effective lifetime estimated by Lange et al. (2022), which makes sense for the effective lifetime is the combination of the chemical lifetime and dispersion lifetime (Lu et al., 2015; De Foy et al., 2014). A significant difference is seen in the summer ~~lifetime estimation~~. Our estimation for summer is 1.1 h, while ~~Zhang et al. (2023) reported an average of 1.4 h, close to the GEOS-Chem model result (Figure 4b, gray line), and we calculate a lower 0.8 h, even lower than the 2—3 h calculated by Liu et al. (2016) for the warm season. We see much more substantial seasonal difference than~~ Lange et al. (2022) reported an ~2 h. ~~.~~ With the known ~~We estimate an average of 5.3 h in winter lifetime and less than one h in summer, while the values are three h in winter and around 2 h for summer, as calculated by Lange et al. (2022). The GEOS-Chem results are between ours and those from Lange et al. (2022), with 4.6 h in winter and 1.3 h in summer. Our calculation is closer to the GEOS-Chem simulation, especially in winter.~~

~~Given the~~ observed satellite NO_2 line densities, the estimated lifetime ~~NO_x emissions~~ will be ~~higher~~ shorter when the estimated NO_x emissions~~lifetime~~ is ~~shorter~~higher, and the estimated ~~emissions lower~~lifetime shorter otherwise (Jin et al., 2021). Thereby, the reasons to explain the higher summer-to-winter NO_x emission ratio can also be used to explain the shorter summer NO_x lifetime in this study.~~Therefore, we estimate higher summer NO_x emissions over Wuhan and lower winter emissions than Lange et al. (2022), leading to a much higher (also more realistic, considering the sectoral emission contributions) summer-to-winter emission ratio in this study. In this work, the a priori NO_x emissions are used to restrict the computation of NO_x emissions. Thereby, we have partly avoided the possible underestimation of NO_x emissions. This may also partly explain the much higher summer-to-winter NO_x emission ratio in this work than in Lange et al. (2022), for they may have underestimated summer NO_x emissions over Wuhan.~~

3.2.3 Interannual variation

Stringent emission control strategies have been implemented in China to control NO_x emissions to combat air pollution since as early as 2010, and a nationwide NO_x emission reduction has been seen since 2012 (Zheng et al., 2018; Li et al., 2024a)~~, and w~~. We find a similar trend over Wuhan from 2018 to 2023. Our calculation shows a ~~slight~~ n increase ~~(3.1%)~~ in NO_x emissions over Wuhan from 2018 to 2019 (~~Figure~~ Fig. ~~5~~6). The outbreak of COVID-19 in early 2020 led to ~~dramatic~~ strong changes in NO_x emissions. Studies have investigated the reduction in satellite NO_2 columns (Bauwens et al., 2020; Fioletov et al., 2022) and NO_x emissions (e.g. Ding et al., 2020; Zheng et al., 2021a; Lange et al., 2022; Zhang et al., 2021) around the world due to the lockdown restrictions to combat the COVID-19. ~~We have also found a more than 70% decrease in NO_x emissions over Wuhan in early February 2020 .~~ Although Wuhan reopened on 9 April 2020, we define the COVID-19 lockdown-influenced period as 23 January to the end of April, considering the slow recovery of human activities. There are ~~25~~ 27 days with valid NO_x emissions estimation during this period, as shown in ~~Figure~~ Fig. ~~5~~6. We calculated the lowest NO_x emissions of less than 20.0 mol s^{-1} during the lockdown, and the mean NO_x emissions in this period are ~~58~~49% lower than the ~~2019 emission levels~~same period in 2019. The mean emission during the other days in 2020 is comparable to 2019. The EDGAR data does not show decrease in NO_x emissions during the lockdown period, while MEIC reveals ~40% reduction (Fig. 2).

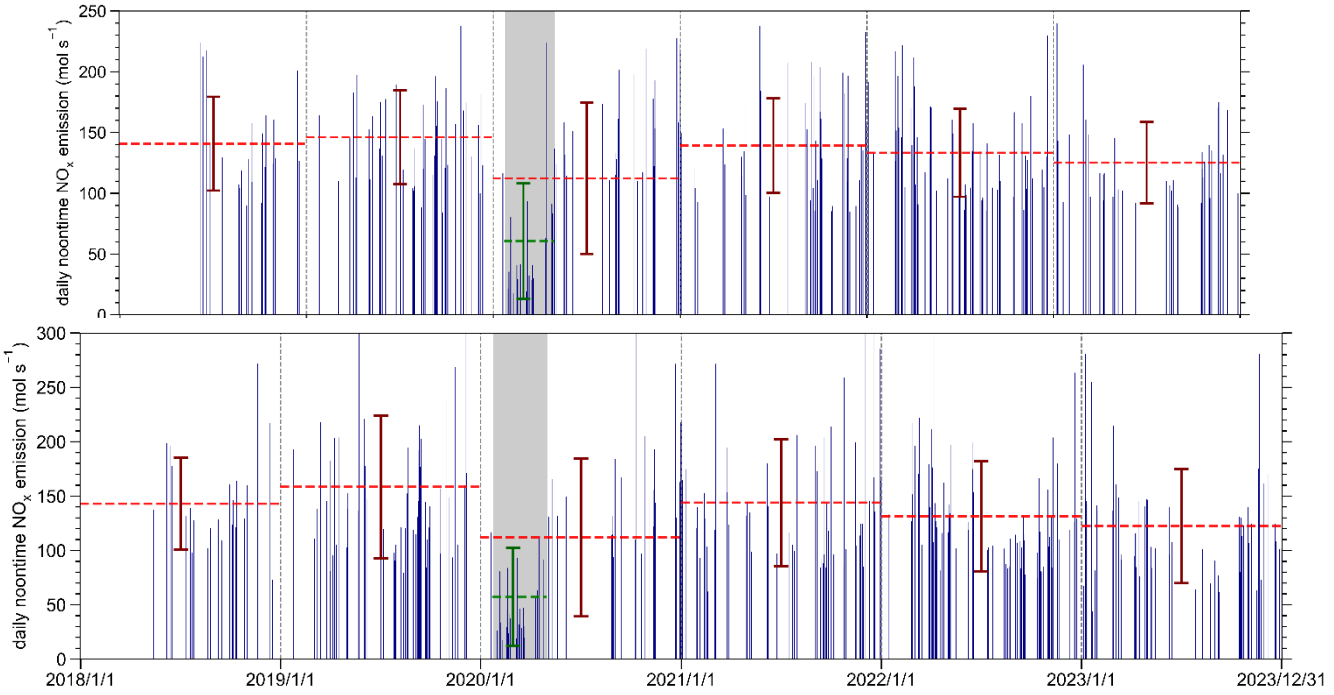

Figure ~~5~~6: Daily ~~NO_x~~ noontime NO_x emissions over Wuhan on ~~clear sky days~~the days with valid estimation from 13 May 2018 through 31 December 2023. The annual mean emissions for each year are marked as red dashed lines~~,~~. ~~and t~~The green dashed line represents the mean NO_x emission during the COVID-19 lockdown-influenced period. The error bars denote the emission standard deviation for each time frame. The COVID-19 lockdown-influenced period is shaded in grey.

We present the estimated annual mean NO_x emissions in Fig. 6, and find a steady decrease after 2019, except the valley in 2020. Considering the strong seasonality of the estimated NO_x emissions and the availability of valid days for calculation in different years, when we make the comparison between two years, the annual mean emissions are calculated based on the months available for both years (Lonsdale and Sun, 2023). For example, January and February estimations are absent for 2019, June and July are not available for 2020, therefore March to May and August to December monthly values are used to determine the annual mean emissions for the comparison of the two years. We find that the estimated NO_x emissions in 2020 is 10.7% lower than 2019, ~~Overall, because of the COVID-19 lockdown, the 2020 annual mean emission is 23.6% below the 2019 level, while~~ Lonsdale and Sun (2023) reported only 5% lower. One possible reason for the difference is that they reported a much higher estimation in October 2020. Emissions in 2021 and 2022 are close to each~~h~~ other and about 10% lower than 2019. A significant decrease (13.6%) is seen in 2023 compared to 2022. ~~emissions over Wuhan in 2020 compared to 2019. NO_x emissions rebound by 21.6% from 2020 to 2021 but are still 7.2% less than the 2019 level. In 2022, we find 9.6% lower NO_x emissions below 2019, while Lonsdale and Sun (2023) reported a larger 26%. A further 6.7% NO_x emission reduction over Wuhan is seen in 2023 under 2022.~~

3.3 Wind field dependence of emission and lifetime estimations

Ideally, NO_x emissions and chemical loss rate directly derived from the satellite observations in combination with the wind fields should be insensitive to the wind direction and even wind speed. However, Valin et al. (2013) showed that the chemical NO_x lifetime in a city plume is wind speed dependent and shorter under strong winds~~. This suggests that it is inappropriate to average the NO_2 plumes at all wind speeds to obtain the mean OH concentration. In our study, we treat every plume separately to estimate the removal rate of NO_x over the city, and this provides us with the opportunity to investigate the dependence of estimated NO_x lifetimes and emissions on the wind direction and speed.~~. The EMG method is found to provide best emission estimation under stronger wind speed condition (De Foy et al., 2014; Ialongo et al., 2014). In this study, we also investigate the superposition column model performance on different wind direction and wind speed groups.~~De Foy et al. (2014)~~

3.3.1 Wind direction

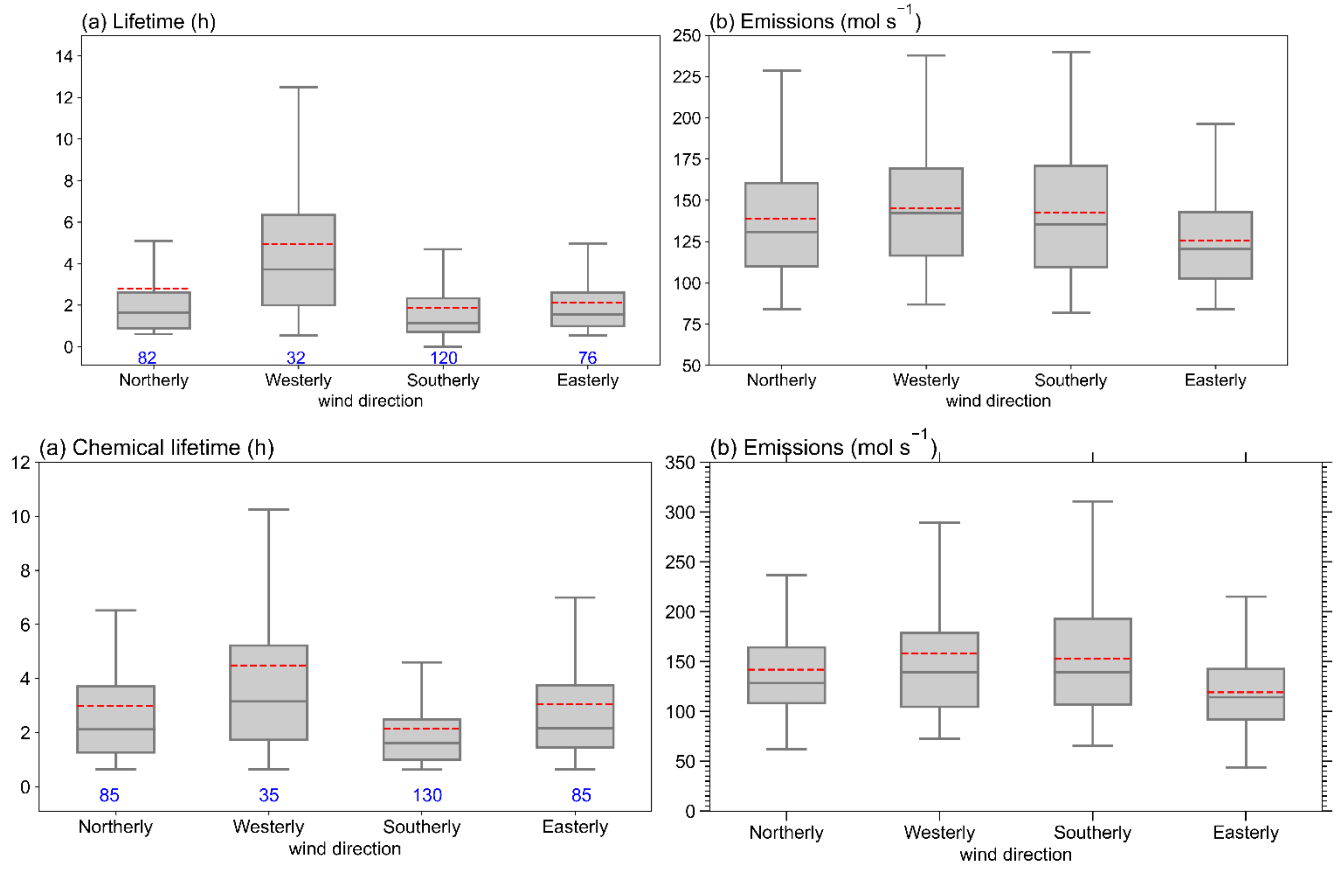

Figure ~~6~~7: Boxplots of estimated NO_x (a) chemical lifetimes and (b) emissions over Wuhan are categorized into four groups based on wind direction. For each box, the middle line indicates the median; the box top and bottom indicate the upper and lower

quartiles, respectively; the whiskers indicate the farthest nonoutlier values; and the means are presented with red dashed lines. The number of days in each category is listed in blue.

We separate the ~~310~~ 345 valid calculations by wind direction (northerly wind: 315 °—45 °, westerly wind: 225 °—315 °, southerly wind: 135 °—225 °, and easterly wind: 45 °—135 °) and compare the estimated NO_x lifetimes and emissions in each category in ~~Figure~~ Fig. ~~6~~7. The variation in NO_x chemical lifetimes with wind direction is closely related to the seasonal prevailing wind direction. About 1/3 of the days with westerly winds are in the winter and more than half of the westerly wind days are in the cold months~~winter winds are from the west~~; consequently, we compute the longest NO_x lifetimes under westerly winds. On the contrary, spring and summer ~~is~~ are dominated by southerly wind, resulting in the shortest NO_x lifetime under this wind direction.

The estimated NO_x emissions also vary with wind directions, as shown in Fig. 7b. Emissions under westerly (southerly) winds are 12% above (8% below) the 345 days' mean emission level, in accordance with the distribution of NO_x chemical lifetimes with the wind direction. ~~We have found in Section 3.2 that the seasonal variation in NO_x emissions is slight in Wuhan. Hence, the dependence of NO_x emission estimation on wind direction is not likely influenced much by the season. We find that NO_x emissions vary little with wind directions, except that estimated NO_x emissions under the easterly wind condition are ~10% lower than the 310 days mean.~~ Both the northerly and easterly winds are most abundant (~50%) in autumn, but estimated emissions under northerly winds are equal to the 345 days' mean level, while it is ~15% lower under the easterly wind. When looking at tropospheric NO_2 columns over Wuhan (~~Figure~~ Fig. ~~1b~~1a), we find that it is relatively clean to the north, west, and south of Wuhan, but there are high NO_2 spots to the east of the city. Although we have tried to avoid the influence of upwind emissions by assuming a linear change in the background NO_2 columns (Zhang et al., 2023), the finding here indicates that it is insufficient. The high NO_2 columns at the starting point of the NO_2 line density will lead to ~~underestimating~~ underestimation of city NO_x emissions; the days with distinct upwind NO_x emissions should be treated cautiously in future calculations.

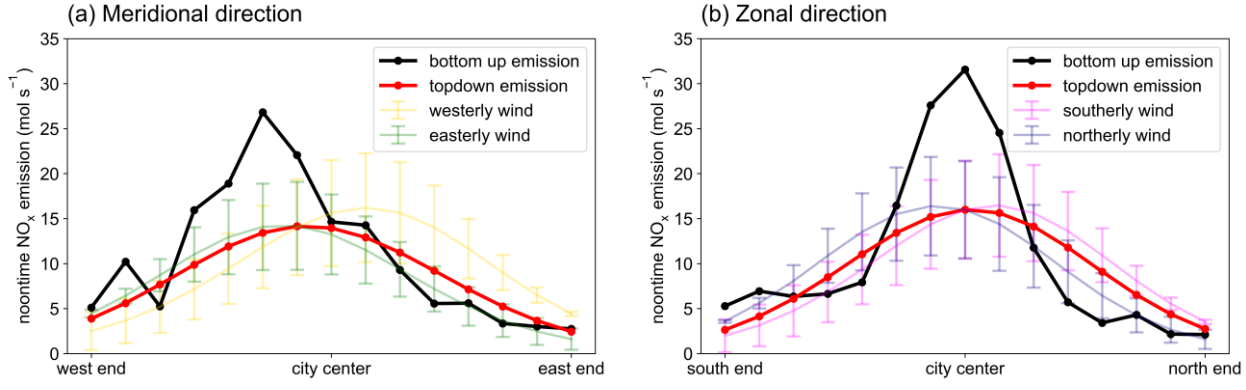

~~**Figure 7: Fitted emission distribution in the (a) meridional direction and (b) zonal direction, the bottom-up emission distribution in the corresponding direction is plotted in a black line.**~~

~~The fitted emission distribution under each wind direction is also compared in Figure 7. We can see clear mirrored distributions between the westerly and easterly wind direction (Figure 7a) and the southerly and northerly wind direction (Figure 7b). This can be explained by the fact that the windy conditions disperse quickly NO_2 away to the downwind region (Goldberg et al., 2024). Finally, the fitted emission distribution in the zonal and meridional directions are basically in line with those from the bottom-up emission inventory, with the difference that the fitted emission distributions are flatter.~~

3.3.2 Wind speed

We then sort our ~~310~~ 345 days with valid NO_x emission calculations into four categories according to wind speed: slow wind (0–3 m s^{-1}), medium slow wind (3–5 m s^{-1}), medium fast wind (5–7 m s^{-1}), and fast wind (> 7 m s^{-1}). We have more than ~~27~~ 23 valid calculations for each category, and the corresponding lifetime and NO_x emissions are shown in ~~Figure~~ Fig. 8. ~~We find that NO_x lifetimes change little when wind speed is less than 7 m s^{-1}, varying from 2.4 h (5–7 m s^{-1}) to 2.6 h (0–3 m s^{-1}). However, a 32% shorter NO_x lifetime at fast wind speed (> 7 m s^{-1}) is seen compared to the slow wind speed (< 5 m s^{-1}), in accordance with the 31% difference calculated by Valin et al. (2013).~~

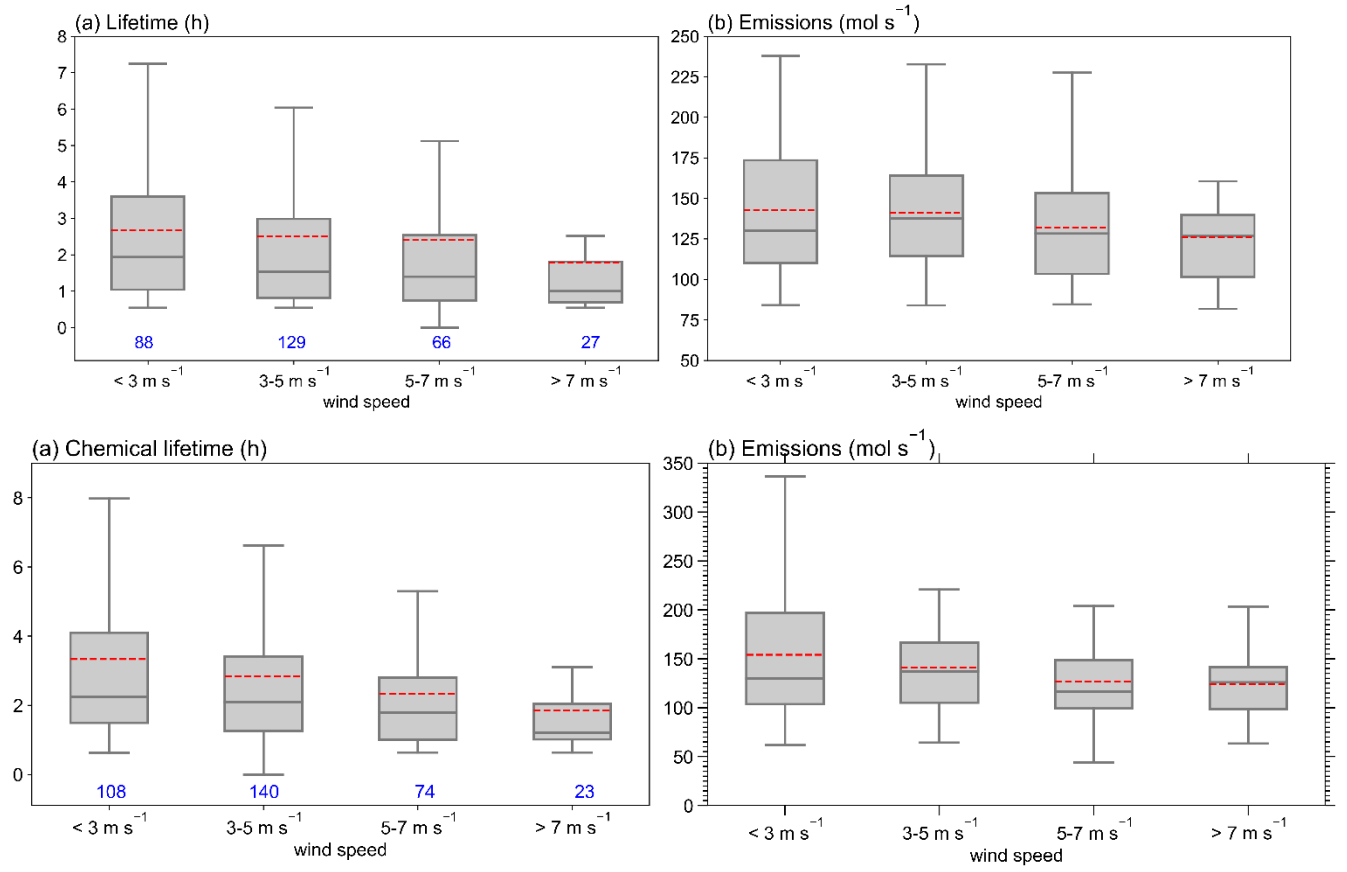

Figure ~~88~~: Same as ~~Figure~~ Fig. ~~6~~ 7 but with the wind speed.

Overall we find a decrease of NO_x chemical lifetime and emission with the increase of the wind speed, which can ~~We find that NO_x lifetimes change little when wind speed is less than 7 m s^{-1}, varying from 2.4 h (5–7 m s^{-1}) to 2.6 h (0–3 m s^{-1}). However, a 32% shorter NO_x lifetime at fast wind speed (> 7 m s^{-1}) is seen compared to the slow wind speed (< 5 m s^{-1}), in accordance with the 31% difference calculated by Valin et al. (2013).~~ ~~Surprisingly, we also estimate slightly lower (about 9%) NO_x emissions when wind speed is fast. It may~~ be explained that the fast wind speed leads to strong ventilation of NO_2 ~~and, thus, lower estimated NO_x emissions~~. Estimated NO_x chemical lifetime decrease by 14—20% as the wind speed increases (Fig. 8a). The lifetime under fast wind is nearly 40% lower than that when the wind speed is slower than 5 m s^{-1}, in accordance with the 31% difference calculated by Valin et al. (2013). The change of estimated NO_x emissions with wind speed is smaller (Fig. 8b). The estimated NO_x emission decreases by ~20% from < 3 to 5—7 m s^{-1} wind speed category, and the emission changes little when wind speed is greater than 5 m s^{-1}. Thus the superposition column underestimate NO_x emissions and chemical lifetimes when the wind speed is faster than 5—7 m s^{-1}. The underestimation rate depends on the fraction of days with fast speed, in Wuhan's case, the overall influence is less than 4% for emission and ~8% for chemical lifetimes.

Then we look back to the varying estimated NO_x emissions in different seasons and under different wind directions. The average wind speeds in the four seasons change small from 3.8 to 4.8 m s^{-1}, falling into the 3—5 m s^{-1} wind speed group. This indicates that the lower summer-to-winter NO_x emission ratio estimated by the top-down method (this study and Lange et al. (2022)) than the bottom-up emission inventories cannot be attributed to the decreasing estimation with the wind speed. In addition, the average wind speeds in the four directions vary from 3.5 to 4.5 m s^{-1}, eliminating the influence of the decreasing estimation with the wind speed on the lower estimated emissions under easterly winds. ~~It has a small influence (less than 1% in Wuhan's case) on the overall estimation of city NO_x emissions, for the days with fast wind make up only less than 10% of the total number of days. The low bias should be considered for cities with a large proportion of fast winds.~~

4 Discussion on the uncertainty

We use the superposition column model to estimate city NO_x emissions and chemical lifetimes on daily basis, and the results are used to analyse the temporal variability of NO_x emissions over Wuhan. There are factors leading to uncertainties in our estimation and analysis.

~~3.3.3 Uncertainties~~

The uncertainties of NO_x emissions and lifetimes estimation come from the parameters and quantities used during the fitting procedure. The primary sources of uncertainties include:

—The systematic error in TROPOMI NO_2 data. The TROPOMI version 2.4.0—2.6.0 data made significant improvements from the earlier versions, and there is a ~20% difference compared to the ground-based data at the Xianghe site in North China (Keppens and Lambert, 2023); we have corrected the possible underestimation over Wuhan by a factor of 1.2, but we thus we still conservatively consider a 20% uncertainty in the NO_2 column.

~~—The bias in the a priori OH concentration. In our previous work (Zhang et al., 2023), we limited the OH concentration between the 0.8—1.2 interval of GEOS-Chem simulated OH concentration and found that the estimated OH concentration in more than 90% of the days fell in this interval, so we exerted a 20% uncertainty on OH concentration. In this study, we conservatively choose the uncertainty of 30% following Lange et al. (2022).~~

—~~Influence of u~~Upwind emissions. ~~Previous work using the superposition column model (Lorente et al., 2019; Zhang et al., 2023) did not consider the influence of NO_x emissions in the surrounding area on the estimation of city NO_x emissions. In this work, w~~We find a ~~10~~15% anomaly in estimated NO_x emission and 8% anomaly in NO_x chemical lifetime for Wuhan when there are distinct hotspots of NO_2 in the upwind region. We thus take the ~~10~~15% (for emission) and 8% (for chemical lifetime) uncertainty to represent the influence of upwind emissions. We must clarify that this part of the uncertainty is 'city-specific~~.~~'. It can be neglected for some isolated cities or large point sources like Paris or Riyadh. For other cities located in polluted backgrounds, the uncertainty in~~tro~~duced by upwind emissions should be calculated accordingly, and it is not necessarily to be ~~10~~15% and 8%.~~.~~

—Bottom-up NO_x emissions~~,~~. We use bottom-up emissions to constrain our estimations. ~~the NO_x/NO_2 ratio, and the wind fields.~~Uncertainty in bottom-up emission inventory is 35% (Zhao et al., 2013; Li et al., 2024b), and we have found that it has a 10% influence on the estimated NO_x emissions while 30% on the chemical lifetime estimation.

—~~as stated in Sect. 2.3. Uncertainty arising from~~ The NO_x/NO_2 ratio ~~and the wind field~~. Uncertainty arises from the NO_x/NO_2 ratio is 10% ~~are 10% and 20%, respectively~~, in accordance with ~~those~~ that from Zhang et al. (2023).

—Wind fields. Uncertainty caused by the wind fields partly comes from the systematic wind error, which we take 20% following Zhang et al. (2023); the other part comes from the limitation of the superposition column model, and we exert 4% for emission and 8% for chemical lifetime estimation. This part of uncertainty is also 'city-specific', and the uncertainty increases as the mean wind speed increases in the study domain. ~~the NO_x/NO_2 ratio, and the wind fields.~~

Finally, we use the root-mean-square sum of all the above contributions, resulting in a ~~54~~35% uncertainty for the NO_x emissions and 44% for NO_x chemical lifetimes estimated for Wuhan.

~~To be mentioned,~~It is noteworthy that Zhang et al. (2023) ~~also~~ considered the uncertainty caused by the area of the study domain and the chemical transport model simulated OH concentration, and they found a 15% and 20% uncertainty caused by the ~~domain size~~two factors, separately. In this study, we leave out the consideration of the uncertainty caused by the size of the study domain because our study domain is limited to the urban area of Wuhan, and it is a proper size to estimate NO_x emissions in the urban area. we discard the model simulated OH concentration in the fitting procedure so the uncertainty caused by the OH concentration is avoided. ~~we leave out the consideration of this part of the uncertainty source because our~~

~~study domain is limited to the urban area of Wuhan, and it is a proper size to estimate NO_x emissions in the urban area.~~We give initial guess of the NO_x chemical lifetimes, the uncertainty of which is not considered because we let it vary in a quite large range, the initial value would have little influence on the fitting.

Our analysis of the temporal variability of the estimated NO_x chemical lifetime and emission is also of uncertainty, though this part of uncertainty is difficult to quantify. First, our conclusion about the insignificant weekly effect of NO_x emission over Wuhan might be reliable, for this is also found in the surface NO_2 and O_3 concentration ~~(references)~~(Wei et al., 2022; Yang et al., 2020), indicating no significant wee~~or~~kday/weekend difference in the oxidation environment. Second, we have overestimated the summer-to-winter emission ratio (0.77), though it is even higher in the bottom-up emission inventory. ~~For one reason, for all the seasons and pollution levels However, the low bias of TROPOMI data is found to be stronger during polluted period (references), which happens more frequently in winter(Douros et al., 2023; Wang et al., 2022), so the fixed scale factor will flatten the seasonal pattern.~~ For one reason, ~~For another, a~~as we have stated in Section 3.2.2, ~~the~~we use a fixed NO_x/NO_2 ratio, which is found to be lower in summer than winter, so the fixed value will lead to ~~we use during the fitting also leads to~~ lower estimated summer-to-winter emission ratio. For another, even though the v2.3.1 and after versions have higher retrieval in winter and over polluted area (Van Geffen et al., 2022), they are still found to be lower in polluted area and higher in clean area, when compared to the ground measurements (Keppens and Lambert, 2023). As a consequence, we may still underestimate winter emissions and/or even overestimate summer emissions, thus leading to a higher estimated summer-to-winter emission ratio. Third, when comparing two years' emissions, the annual mean emissions are calculated based on the months available for both years instead of all valid days' average. In this way we have minimized the uncertainty caused by the different availability of valid days in different years. However, the reliability of our results need more years of estimation and more bottom-up information to confirm. ~~Fourth, based on the analysis of wind direction dependence of the estimated NO_x chemical lifetime and emission, we point out the limitation of the superposition column model of underestimating NO_x emissions when there is emission hotspot in the upwind direction. The 15% underestimation is determined for the city of Wuhan, but we need more estimation for this city and others to confirm this uncertainty rate. Finally, we find that fast wind speed (>7 m s^{-1}) leads to 40% lower NO_x chemical lifetime estimation.~~

~~4~~ 5 Conclusion

In this work, we use the superposition column model to calculate city NO_x emissions and lifetimes on a daily basis, with a time span of nearly six years, from May 2018 to December 2023. The city of Wuhan is used as an example to investigate the seasonal pattern, weekly cycle, and interannual variation of city NO_x emissions. The dependence of ~~estimated NO_x emissions and lifetimes~~the model performance on the wind direction and speed are also discussed. We choose the urban area of Wuhan as our study domain, about ~~90 km in diameter~~45 km radium around the city center. For each ~~clear sky day~~full-NO_2-coverage day with a homogeneous wind field, the TROPOMI NO_2 columns are sampled in to a ~~we sample the TROPOMI NO_2 column data in~~ 15 × 15 grid that is align with the wind direction~~the grid size of 6 km × 6 km and rotate it with the wind~~

~~direction~~. Then, every 15 grid cells perpendicular to the wind direction are accumulated to form the NO_2 line density. The NO_2 line density is fitted with the superposition column model to obtain the final daily NO_x emissions and lifetimes.

For the period from May 2018 to December 2023, we obtain ~~335~~ 372 days with valid NO_x emissions and lifetimes estimations over Wuhan, with more than ~~50~~ 60 days for each season and each year (2018 excepted) and more than 40 days for each ~~weekday and weekends~~day of the week. The monthly NO_x emissions ~~for the years 2018 and 2019~~from 2018 to 2022 are compared with those from EDGAR v8.1 and ~~ABACAS~~ MEIC v1.4 (until 2020) bottom-up emission inventories~~, respectively~~. ~~We see 39% lower NO_x emissions over Wuhan compared to the EDGAR v6.1 dataset, and the difference is only 4.7% compared to the ABACAS inventory.~~The difference between our estimation and the bottom-up emissions inventories is within 35% for 2018－2019, and EDGAR v8.1 emission is higher by more than 50% than our estimation in 2020－2022. We find a ~~moderate seasonal variation with a relatively high (~~0.7~~8~~7~~)~~ summer-to-winter NO_x emission ratio, which might be biased high, though it is even higher in the bottom-up inventory (> 0.85). ~~This can partly be explained by the fact that we use the ABACAS bottom-up NO_x emissions as one of the limiting factors to constrain the top-down emissions, avoiding the possible underestimation of NO_x emissions in the summertime when NO_2 columns are rather low.~~ The estimated noontime NO_x lifetimes vary from ~~less than 1~~1.1 h in summer to ~~5.3~~4.1 h in winter, with an average of 2.~~6~~ 8 h. We see ~~only a slight drop in NO_x emissions on weekends (the weekend-to-weekday ratio is 0.95) over~~insignificant weekly cycle for Wuhan, which may be related to the living culture and style of the Chinese. We find that NO_x emissions over Wuhan during the COVID-19 lockdown-influenced period are nearly ~~60~~50% lower than the normal level and rebound to the 2019 emission level for the rest of 2020. Overall, our calculations reveal a steady decline in NO_x emissions from 2019 to 2023~~, and the emissions in 2023 are 15.6% below the 2019 level~~.

Compared to previous studies using the superposition column model (Lorente et al., 2019; Zhang et al., 2023), we discard the CTMs simulated OH concentration in the derivation of NO_x chemical loss rate. By doing so we make this method CTM-independent and computational efficient, and also avoid the uncertainty caused by the OH concentration. We use the bottom-up emission inventory to constrain the emission estimation, which induces about 10% uncertainty to the estimation and leads to overestimation of the summer-to-winter emission ratio.

We separate the ~~310~~ 345 days (~~25~~ 27 days during the COVID-19 lockdown excluded) of NO_x emissions and lifetimes according to wind direction and speed to investigate the model performance under the wind field influence. We find a ~~10~~15% lower estimated NO_x emissions in the condition with distinct upwind emissions, indicating that we need to be more careful in the future when computing NO_x emissions over cities or large point sources located in a polluted background. Because of the ventilation of NO_2 under fast wind speed, the estimated NO_x chemical lifetime and emission decrease as the wind speed increases. Thereby, the estimation will be underestimated for the sources dominated with fast winds. ~~We also see 30% shorter NO_x lifetime under fast wind.~~

We have demonstrated in this work that by combining the superposition column model and the high spatial resolution TROPOMI NO_2 column product, one can investigate the variability of NO_x emissions and lifetimes on daily to annual time

scale. We also provide recommendations for dealing with conditions with upwind emissions and high wind speeds for better and more accurate city NO_x emissions estimations. So far, the superposition column model has only been used for two cities, Paris and Wuhan; we will extend it to other cities and emission sources in the future.

Author contributions. QZ and KFB designed the research. QZ did the processing, visualizations and main writing. KFB edited the paper. CL and AM provided improvements in the method. BZ and SL provided the ABACAS emission inventory. YP reviewed the paper.

Competing interests. The authors declare no competing financial interest.

Acknowledgement. This work is supported by the National Natural Science Foundation of China (grant no. 42375106 and 41805098) and the National Key R&D Program of China (No. 2023YFB3907500). The Copernicus Sentinel-5P level-2 NO_2 data are employed in this work. Sentinel-5 Precursor is a European Space Agency (ESA) mission on behalf of the European Commission (EC). The TROPOMI payload is a joint development by ESA and the Netherlands Space Office. The Sentinel-5 Precursor ground segment development has been funded by ESA and with national contributions from the Netherlands, Germany, and Belgium. The ~~Wind~~ wind fields used in this study are provided by ECMWF ERA5. EDGAR ~~v6~~v8.1 Global Air Pollutant Emissions are provided by https://edgar.jrc.ec.europa.eu/dataset_ap81 ~~https://edgar.jrc.ec.europa.eu/dataset_ap61~~ (last access: ~~13~~ 2 ~~September~~ December 2024). We Thank Professor Qiao Ma from Shandong University for performing the comparison between result from this study and the MEIC v1.4 emission inventory.

Data availability. The TROPOMI NO_2 data can be freely downloaded from the Tropospheric Emission Monitoring Internet Service (https://www.temis.nl/airpollution/no2.php). The ERA5 data can be found at the Copernicus Climate Change (C3S) climate data store (CDS) (https://cds.climate.copernicus.eu/cdsapp#!/dataset/reanalysis-era5-pressure-levels?tab=overview).

References

, !!! INVALID CITATION !!! (Zhang et al., 2021).

Baklanov, A., Molina, L. T., and Gauss, M.: Megacities, air quality and climate, Atmospheric Environment, 126, 235-249, 10.1016/j.atmosenv.2015.11.059, 2016.

Bassett, M. and Seinfeld, J. H.: Atmospheric equilibrium model of sulfate and nitrate aerosols, Atmospheric Environment, 17, 2237-2252, https://doi.org/10.1016/0004-6981(83)90221-4, 1983.

Bauwens, M., Compernolle, S., Stavrakou, T., Muller, J. F., van Gent, J., Eskes, H., Levelt, P. F., van der, A. R., Veefkind, J. P., Vlietinck, J., Yu, H., and Zehner, C.: Impact of coronavirus outbreak on NO_2 pollution assessed using TROPOMI and OMI observations, Geophysical Research Letters, 47, e2020GL087978, 10.1029/2020GL087978, 2020.

Beirle, S., Platt, U., Wenig, M., and Wagner, T.: Weekly cycle of NO_2 by GOME measurements: a signature of anthropogenic sources, Atmospheric Chemistry and Physics, 3, 2225-2232, doi: 10.5194/acp-3-2225-2003, 2003.

Beirle, S., Boersma, K. F., Platt, U., Lawrence, M. G., and Wagner, T.: Megacity emissions and lifetimes of nitrogen oxides probed from space, Science, 333, 1737-1739, 10.1126/science.1207824, 2011.
Beirle, S., Borger, C., Dorner, S., Li, A., Hu, Z., Liu, F., Wang, Y., and Wagner, T.: Pinpointing nitrogen oxide emissions from space, Science Advances, 5, eaax9800, doi: 10.1126/sciadv.aax9800, 2019.
Bovensmann, H., Burrows, J. P., Buchwitz, M., Frerick, J., Noel, S., Rozanov, V., Chance, K., and Goede, A.: SCIAMACHY: Mission Objectives and Measurement Modes, Journal of the Atmospheric Sciences, 56, 127-150, 1999.
Burrows, J. P., Weber, M., Buchwitz, M., Rozanov, V., Ladstatter-Weibenmayer, A., Richter, A., DeBeek, R., Hoogen, R., Bramstedt, K., Eichmann, K.-U., Eisinger, M., and Perner, D.: The Global Ozone Monitoring Experiment (GOME): Mission Concept and First Scientific Results, Journal of the Atmospheric Sciences, 56, 151-175, https://doi.org/10.1175/1520-0469(1999)056<0151:TGOMEG>2.0.CO;2, 1999.
Butler, T. M., Lawrence, M. G., Gurjar, B. R., van Aardenne, J., Schultz, M., and Lelieveld, J.: The representation of emissions from megacities in global emission inventories, Atmospheric Environment, 42, 703-719, 10.1016/j.atmosenv.2007.09.060, 2008.
de Foy, B., Lu, Z., Streets, D. G., Lamsal, L. N., and Duncan, B. N.: Estimates of power plant NO_x emissions and lifetimes from OMI NO_2 satellite retrievals, Atmospheric Environment, 116, 1-11, 10.1016/j.atmosenv.2015.05.056, 2015.
de Foy, B., Wilkins, J. L., Lu, Z., Streets, D. G., and Duncan, B. N.: Model evaluation of methods for estimating surface emissions and chemical lifetimes from satellite data, Atmospheric Environment, 98, 66-77, 10.1016/j.atmosenv.2014.08.051, 2014.
Ding, J., van der A, R. J., Mijling, B., and Levelt, P. F.: Space-based NO_x emission estimates over remote regions improved in DECSO, Atmospheric Measurement Techniques, 10, 925-938, 10.5194/amt-10-925-2017, 2017.
Ding, J., van der A, R. J., Eskes, H. J., Mijling, B., Stavrakou, T., Geffen, J. H. G. M., and Veefkind, J. P.: NO_x Emissions Reduction and Rebound in China Due to the COVID-19 Crisis, Geophysical Research Letters, 47, e2020GL089912, 10.1029/2020gl089912, 2020.
Douros, J., Eskes, H., van Geffen, J., Boersma, K. F., Compernolle, S., Pinardi, G., Blechschmidt, A.-M., Peuch, V.-H., Colette, A., and Veefkind, P.: Comparing Sentinel-5P TROPOMI NO2 column observations with the CAMS regional air quality ensemble, Geoscientific Model Development, 16, 509-534, 10.5194/gmd-16-509-2023, 2023.
Eskes, H., Eichmann, K.-U., Lambert, J.-C., Loyola, D. G., Stein-Zweers, D., Dehn, A., and Zehner, C.: S5P MPC Product Readme Nitrogen Dioxide, https://doi.org/10.5270/S5P-9bnp8q8, 2023.
Fioletov, V., McLinden, C. A., Griffin, D., Krotkov, N., Liu, F., and Eskes, H.: Quantifying urban, industrial, and background changes in NO_2 during the COVID-19 lockdown period based on TROPOMI satellite observations, Atmospheric Chemistry and Physics, 22, 4201-4236, 10.5194/acp-22-4201-2022, 2022.
Geng, G., Zhang, Q., Tong, D., Li, M., Zheng, Y., Wang, S., and He, K.: Chemical composition of ambient $PM_{2.5}$ over China and relationship to precursor emissions during 2005–2012, Atmospheric Chemistry and Physics, 17, 9187-9203, 10.5194/acp-17-9187-2017, 2017.
Goldberg, D. L., Anenberg, S. C., Kerr, G. H., Mohegh, A., Lu, Z., and Streets, D. G.: TROPOMI NO_2 in the United States: A Detailed Look at the Annual Averages, Weekly Cycles, Effects of Temperature, and Correlation With Surface NO_2 Concentrations, Earth's Future, 9, e2020EF001665, doi: 10.1029/2020EF001665, 2021a.
Goldberg, D. L., Anenberg, S. C., Lu, Z., Streets, D. G., Lamsal, L. N., McDuffie, E. E., and Smith, S. J.: Urban NO_x emissions around the world declined faster than anticipated between 2005 and 2019, Environmental Research Lettters, 16, 115004, doi: 10.1088/1748-9326/ac2c34, 2021b.
Goldberg, D. L., Lu, Z., Streets, D. G., De Foy, B., Griffin, D., Mclinden, C. A., Lamsal, L. N., Krotkov, N. A., and Eskes, H.: Enhanced capabilities of TROPOMI NO_2: estimating NO_x from North American cities and power plants, Environmental Science & Technology, 53, 12594-12601, 10.1021/acs.est.9b04488, 2019.
Goldberg, D. L., Tao, M., Kerr, G. H., Ma, S., Tong, D. Q., Fiore, A. M., Dickens, A. F., Adelman, Z. E., and Anenberg, S. C.: Evaluating the spatial patterns of U.S. urban NOx emissions using TROPOMI NO_2, Remote Sensing of Environment, 300, 10.1016/j.rse.2023.113917, 2024.
Hersbach, H., Bell, B., Berrisford, P., Hirahara, S., Horányi, A., Muñoz-Sabater, J., Nicolas, J., Peubey, C., Radu, R., Schepers, D., Simmons, A., Soci, C., Abdalla, S., Abellan, X., Balsamo, G., Bechtold, P., Biavati, G., Bidlot, J., Bonavita, M., Chiara, G., Dahlgren, P., Dee, D., Diamantakis, M., Dragani, R., Flemming, J., Forbes, R., Fuentes, M., Geer, A., Haimberger, L., Healy, S., Hogan, R. J., Hólm, E., Janisková, M., Keeley, S., Laloyaux, P., Lopez, P., Lupu, C., Radnoti, G., Rosnay, P., Rozum, I., Vamborg, F., Villaume, S., and Thépaut, J. N.: The ERA5 global reanalysis, Quarterly Journal of the Royal Meteorological Society, 146, 1999-2049, 10.1002/qj.3803, 2020.
Ialongo, I., Hakkarainen, J., Hyttinen, N., Jalkanen, J.-P., Johansson, L., Boersma, F., Krotkov, N., and Tamminen, J.: Characterization of OMI tropospheric NO_2 over the Baltic Sea region, Atmospheric Chemistry and Physics, 14, 7795-7805, 10.5194/acp-14-7795-2014, 2014.
Jacob, D.: Introduction to Atmospheric Chemistry, Princeton Univ. Press, 1999.
Jin, X., Zhu, Q., and Cohen, R. C.: Direct estimates of biomass burning NO_x emissions and lifetimes using daily observations from TROPOMI, Atmospheric Chemistry and Physics, 21, 15569-15587, 10.5194/acp-21-15569-2021, 2021.
Keppens, A. and Lambert, J.-C.: Quarterly Validation Report of the Copernicus Sentinel-5 Precursor Operational Data Products #21: April 2018 - November 2023, https://mpc-vdaf.tropomi.eu, 2023.

Kharol, S. K., Martin, R. V., Philip, S., Boys, B., Lamsal, L. N., Jerrett, M., Brauer, M., Crouse, D. L., McLinden, C., and Burnett, R. T.: Assessment of the magnitude and recent trends in satellite-derived ground-level nitrogen dioxide over North America, Atmospheric Environment, 118, 236-245, 10.1016/j.atmosenv.2015.08.011, 2015.

Kong, H., Lin, J., Zhang, R., Liu, M., Weng, H., Ni, R., Chen, L., Wang, J., Yan, Y., and Zhang, Q.: High-resolution (0.05° × 0.05°) NO_x emissions in the Yangtze River Delta inferred from OMI, Atmospheric Chemistry and Physics, 19, 12835-12856, 10.5194/acp-19-12835-2019, 2019.

Lamsal, L. N., Martin, R. V., Padmanabhan, A., van Donkelaar, A., Zhang, Q., Sioris, C. E., Chance, K., Kurosu, T. P., and Newchurch, M. J.: Application of satellite observations for timely updates to global anthropogenic NO_x emission inventories, Geophysical Research Letters, 38, L05810, doi: 10.1029/2010gl046476, 2011.

Lange, K., Richter, A., and Burrows, J. P.: Variability of nitrogen oxide emission fluxes and lifetimes estimated from Sentinel-5P TROPOMI observations, Atmospheric Chemistry and Physics, 22, 2745-2767, doi: 10.5194/acp-22-2745-2022, 2022.

Lange, K., Richter, A., Schönhardt, A., Meier, A. C., Bösch, T., Seyler, A., Krause, K., Behrens, L. K., Wittrock, F., Merlaud, A., Tack, F., Fayt, C., Friedrich, M. M., Dimitropoulou, E., Van Roozendael, M., Kumar, V., Donner, S., Dörner, S., Lauster, B., Razi, M., Borger, C., Uhlmannsiek, K., Wagner, T., Ruhtz, T., Eskes, H., Bohn, B., Santana Diaz, D., Abuhassan, N., Schüttemeyer, D., and Burrows, J. P.: Validation of Sentinel-5P TROPOMI tropospheric NO2 products by comparison with NO2 measurements from airborne imaging DOAS, ground-based stationary DOAS, and mobile car DOAS measurements during the S5P-VAL-DE-Ruhr campaign, Atmospheric Measurement Techniques, 16, 1357-1389, 10.5194/amt-16-1357-2023, 2023.

Levelt, P. F., van den Oord, G. H. J., Dobber, M. R., Malkki, A., Huib, V., Johan de, V., Stammes, P., Lundell, J. O. V., and Saari, H.: The ozone monitoring instrument, IEEE Transactions on Geoscience and Remote Sensing, 44, 1093-1101, doi: 10.1109/tgrs.2006.872333, 2006.

Li, H., Zheng, B., Lei, Y., Hauglustaine, D., Chen, C., Lin, X., Zhang, Y., Zhang, Q., and He, K.: Trends and drivers of anthropogenic NO emissions in China since 2020, Environmental Science and Ecotechnology, 21, 10.1016/j.ese.2024.100425, 2024a.

Li, K., Jacob, D. J., Liao, H., Zhu, J., Shah, V., Shen, L., Bates, K. H., Zhang, Q., and Zhai, S.: A two-pollutant strategy for improving ozone and particulate air quality in China, Nature Geoscience, 12, 906-910, 10.1038/s41561-019-0464-x, 2019.

Li, M., Kurokawa, J., Zhang, Q., Woo, J.-H., Morikawa, T., Chatani, S., Lu, Z., Song, Y., Geng, G., Hu, H., Kim, J., Cooper, O. R., and McDonald, B. C.: MIXv2: a long-term mosaic emission inventory for Asia (2010–2017), Atmospheric Chemistry and Physics, 24, 3925-3952, doi: 10.5194/acp-24-3925-2024, 2024b.

Liu, F., Beirle, S., Zhang, Q., Dörner, S., He, K., and Wagner, T.: NO_x lifetimes and emissions of cities and power plants in polluted background estimated by satellite observations, Atmospheric Chemistry and Physics, 16, 5283-5298, 10.5194/acp-16-5283-2016, 2016.

Liu, F., Tao, Z., Beirle, S., Joiner, J., Yoshida, Y., Smith, S. J., Knowland, K. E., and Wagner, T.: A new method for inferring city emissions and lifetimes of nitrogen oxides from high-resolution nitrogen dioxide observations: a model study, Atmospheric Chemistry and Physics, 22, 1333-1349, 10.5194/acp-22-1333-2022, 2022.

Lonsdale, C. R. and Sun, K.: Nitrogen oxides emissions from selected cities in North America, Europe, and East Asia observed by the TROPOspheric Monitoring Instrument (TROPOMI) before and after the COVID-19 pandemic, Atmospheric Chemistry and Physics, 23, 8727-8748, 10.5194/acp-23-8727-2023, 2023.

Lorente, A., Boersma, K. F., Eskes, H. J., Veefkind, J. P., van Geffen, J., de Zeeuw, M. B., Denier van der Gon, H. A. C., Beirle, S., and Krol, M. C.: Quantification of nitrogen oxides emissions from build-up of pollution over Paris with TROPOMI, Scitific Report, 9, 20033, doi: 10.1038/s41598-019-56428-5, 2019.

Lu, X., Zhang, L., Chen, Y., Zhou, M., Zheng, B., Li, K., Liu, Y., Lin, J., Fu, T.-M., and Zhang, Q.: Exploring 2016–2017 surface ozone pollution over China: source contributions and meteorological influences, Atmospheric Chemistry and Physics, 19, 8339-8361, 10.5194/acp-19-8339-2019, 2019.

Lu, Z., Streets, D. G., de Foy, B., Lamsal, L. N., Duncan, B. N., and Xing, J.: Emissions of nitrogen oxides from US urban areas: estimation from Ozone Monitoring Instrument retrievals for 2005-2014, Atmospheric Chemistry and Physics, 15, 10367-10383, doi: 10.5194/acp-15-10367-2015, 2015.

Martin, R. V., Jacob, D. J., Chance, K., Kurosu, T. P., Palmer, P. I., and Evans, M. J.: Global inventory of nitrogen oxide emissions constrained by space-based observations of NO_2 columns, Journal of Geophysical Research, 108, doi: 10.1029/2003jd003453, 2003.

Park, H., Jeong, S., Park, H., Labzovskii, L. D., and Bowman, K. W.: An assessment of emission characteristics of Northern Hemisphere cities using spaceborne observations of CO_2, CO, and NO_2, Remote Sensing of Environment, 254, 10.1016/j.rse.2020.112246, 2021.

Penner, J. E., Atherton, C. S., Dignon, J., Chan, S. J., and Walton, J. J.: Tropospheric nitrogen: A three-dimensional study of sources, distributions, and deposition, Journal of Geophysical Research, 96, 959-990, https://doi.org/10.1029/90JD02228, 1991.

Rey-Pommier, A., Chevallier, F., Ciais, P., Broquet, G., Christoudias, T., Kushta, J., Hauglustaine, D., and Sciare, J.: Quantifying NO_x emissions in Egypt using TROPOMI observations, Atmospheric Chemistry and Physics, 22, 11505-11527, 10.5194/acp-22-11505-2022, 2022.

Seinfeld, J. H. and Pandis, S. N.: Atmospheric Chemistry and Physics: from air pollution to climate change, Hoboken, New Jersey2016.

Stavrakou, T., Muller, J. F., Bauwens, M., Boersma, K. F., and van Geffen, J.: Satellite evidence for changes in the NO_2 weekly cycle over large cities, Scientific Report, 10, 10066, doi: 10.1038/s41598-020-66891-0, 2020.

Valin, L. C., Russell, A. R., and Cohen, R. C.: Variations of OH radical in an urban plume inferred from NO_2 column measurements, Geophysical Research Letters, 40, 1856-1860, 10.1002/grl.50267, 2013.

van Geffen, J., Boersma, K. F., Eskes, H., Sneep, M., ter Linden, M., Zara, M., and Veefkind, J. P.: S5P TROPOMI NO_2 slant column retrieval: method, stability, uncertainties and comparisons with OMI, Atmospheric Measurement Techniques, 13, 1315-1335, 10.5194/amt-13-1315-2020, 2020.

van Geffen, J., Eskes, H., Compernolle, S., Pinardi, G., Verhoelst, T., Lambert, J.-C., Sneep, M., ter Linden, M., Ludewig, A., Boersma, K. F., and Veefkind, J. P.: Sentinel-5P TROPOMI NO_2 retrieval: impact of version v2.2 improvements and comparisons with OMI and ground-based data, Atmospheric Measurement Techniques, 15, 2037-2060, 10.5194/amt-15-2037-2022, 2022.

Veefkind, J. P., Aben, I., McMullan, K., Förster, H., de Vries, J., Otter, G., Claas, J., Eskes, H. J., de Haan, J. F., Kleipool, Q., van Weele, M., Hasekamp, O., Hoogeveen, R., Landgraf, J., Snel, R., Tol, P., Ingmann, P., Voors, R., Kruizinga, B., Vink, R., Visser, H., and Levelt, P. F.: TROPOMI on the ESA Sentinel-5 Precursor: A GMES mission for global observations of the atmospheric composition for climate, air quality and ozone layer applications, Remote Sensing of Environment, 120, 70-83, 10.1016/j.rse.2011.09.027, 2012.

Visser, A. J., Boersma, K. F., Ganzeveld, L. N., and Krol, M. C.: European NO_x emissions in WRF-Chem derived from OMI: impacts on summertime surface ozone, Atmospheric Chemistry and Physics, 19, 11821-11841, 10.5194/acp-19-11821-2019, 2019.

Wang, C., Wang, T., Wang, P., and Wang, W.: Assessment of the Performance of TROPOMI NO2 and SO2 Data Products in the North China Plain: Comparison, Correction and Application, Remote Sensing, 14, 10.3390/rs14010214, 2022.

Wei, J., Liu, S., Li, Z., Liu, C., Qin, K., Liu, X., Pinker, R. T., Dickerson, R. R., Lin, J., Boersma, K. F., Sun, L., Li, R., Xue, W., Cui, Y., Zhang, C., and Wang, J.: Ground-Level NO_2 Surveillance from Space Across China for High Resolution Using Interpretable Spatiotemporally Weighted Artificial Intelligence, Environmental Science & Technology, 56, 9988-9998, doi: 10.1021/acs.est.2c03834, 2022.

Xing, J., Li, S. M., Zheng, S., Liu, C., Wang, X., Huang, L., Song, G., He, Y., Wang, S., Sahu, S. K., Zhang, J., Bian, J., Zhu, Y., Liu, T.-Y., and Hao, J.: Rapid Inference of nitrogen oxide emissions based on a top-down method with a physically informed variational autoencoder, Environmental Science & Technology, 56, 12, 10.1021/acs.est.1c08337, 2022.

Yang, G., Liu, Y., and Li, X.: Spatiotemporal distribution of ground-level ozone in China at a city level, Scientific Reports, 10, 10.1038/s41598-020-64111-3, 2020.

Zhai, S., Jacob, D. J., Wang, X., Liu, Z., Wen, T., Shah, V., Li, K., Moch, J. M., Bates, K. H., Song, S., Shen, L., Zhang, Y., Luo, G., Yu, F., Sun, Y., Wang, L., Qi, M., Tao, J., Gui, K., Xu, H., Zhang, Q., Zhao, T., Wang, Y., Lee, H. C., Choi, H., and Liao, H.: Control of particulate nitrate air pollution in China, Nature Geoscience, 14, 389-395, 10.1038/s41561-021-00726-z, 2021.

Zhang, L., Liu, L., Zhao, Y., Gong, S., Zhang, X., Henze, D. K., Capps, S. L., Fu, T.-M., Zhang, Q., and Wang, Y.: Source attribution of particulate matter pollution over North China with the adjoint method, Environmental Research Letters, 10, 10.1088/1748-9326/10/8/084011, 2015.

Zhang, Q., Boersma, K. F., Zhao, B., Eskes, H., Chen, C., Zheng, H., and Zhang, X.: Quantifying daily NO_x and CO_2 emissions from Wuhan using satellite observations from TROPOMI and OCO-2, Atmospheric Chemistry and Physics, 23, 551-563, doi: 10.5194/acp-23-551-2023, 2023.

Zhang, Q., Pan, Y., He, Y., Walters, W. W., Ni, Q., Liu, X., Xu, G., Shao, J., and Jiang, C.: Substantial nitrogen oxides emission reduction from China due to COVID-19 and its impact on surface ozone and aerosol pollution, Science of The Total Environment, 753, 142238, 10.1016/j.scitotenv.2020.142238, 2021.

Zhao, B., Wang, S. X., Liu, H., Xu, J. Y., Fu, K., Klimont, Z., Hao, J. M., He, K. B., Cofala, J., and Amann, M.: NO_x emissions in China: historical trends and future perspectives, Atmospheric Chemistry and Physics, 13, 9869-9897, 10.5194/acp-13-9869-2013, 2013.

Zhao, B., Zheng, H., Wang, S., Smith, K. R., Lu, X., Aunan, K., Gu, Y., Wang, Y., Ding, D., Xing, J., Fu, X., Yang, X., Liou, K. N., and Hao, J.: Change in household fuels dominates the decrease in $PM_{2.5}$ exposure and premature mortality in China in 2005-2015, Proceedings of the National Academy of Sciences, 115, 12401-12406, 10.1073/pnas.1812955115, 2018.

Zheng, B., Zhang, Q., Geng, G., Chen, C., Shi, Q., Cui, M., Lei, Y., and He, K.: Changes in China's anthropogenic emissions and air quality during the COVID-19 pandemic in 2020, Earth System Science Data, 13, 2895-2907, 10.5194/essd-13-2895-2021, 2021a.

Zheng, B., Cheng, J., Geng, G., Wang, X., Li, M., Shi, Q., Qi, J., Lei, Y., Zhang, Q., and He, K.: Mapping anthropogenic emissions in China at 1 km spatial resolution and its application in air quality modeling, Science Bulletin, 66, 612-620, 10.1016/j.scib.2020.12.008, 2021b.

Zheng, B., Tong, D., Li, M., Liu, F., Hong, C., Geng, G., Li, H., Li, X., Peng, L., Qi, J., Yan, L., Zhang, Y., Zhao, H., Zheng, Y., He, K., and Zhang, Q.: Trends in China's anthropogenic emissions since 2010 as the consequence of clean air actions, Atmospheric Chemistry and Physics, 18, 14095-14111, doi: 10.5194/acp-18-14095-2018, 2018.

Zheng, H., Zhao, B., Wang, S., Wang, T., Ding, D., Chang, X., Liu, K., Xing, J., Dong, Z., Aunan, K., Liu, T., Wu, X., Zhang, S., and Wu, Y.: Transition in source contributions of $PM_{2.5}$ exposure and associated premature mortality in China during 2005-2015, Environment International, 132, 105111, 10.1016/j.envint.2019.105111, 2019.